56 $[(CH_3)_2NH_2]_3Sb_2Cl_9$ family

56A Pure compounds

No. 56A-1 $[(CH_3)_2NH_2]_3Sb_2Cl_9$, Dimethylammonium nonachlorodiantimonate

(M = 700.85)

1a	Ferroelectric activity in $[(CH_3)_2NH_2]_3Sb_2Cl_9$ was discovered by Jakubas in 1986.			86Jak
b	phase	II	I	86Jak
	state	F	P	
	crystal system	monoclinic	monoclinic	
	space group	Pa $-C_s^{2}$ [a])	$P2_1/a$ $-C_{2h}^{5}$ [b])	[a]) 96Zal
	Θ [K]	242		[b]) 88Gda
	Cleavage plane is nearly perpendicular to the c axis.			86Jak
	Ferroelectric axis is close to the a axis and slightly deflected from the a–b cleavage plane.			86Jak
	$\rho = 1.89 \cdot 10^3$ kg m^{-3}.			86Jak
	$\rho_X = 1.91 \cdot 10^3$ kg m^{-3}.			88Gda
2a	Crystal growth: evaporation method from the stoichiometric aqueous solution of Sb_2O_3 and $[(CH_3)_2NH_2]Cl$ at a high excess of HCl.			86Jak
3a	Unit cell parameters:			
	Phase I: a = 14.045(4) Å, b = 9.018(3) Å, c = 9.670(2) Å, β = 95.47(2)° at 301 K.			88Gda
	Phase II: a = 14.080(4) Å, b = 9.034(3) Å, c = 9.470(3) Å, β = 95.81(3)° at 200 K.			96Zal
b	Z = 2 in phases I and II.			86Jak, 96Zal
	Crystal structure: Fig. 56A-1-001, Fig. 56A-1-002, Fig. 56A-1-003, Fig. 56A-1-004, Fig. 56A-1-005, Fig. 56A-1-006.			
	Positional and temperature parameters: Table 56A-1-001, Table 56A-1-002, Table 56A-1-003, Table 56A-1-004.			
	Interatomic distances and bond angles: Table 56A-1-005, Table 56A-1-006, Table 56A-1-007.			
	Bond distances and angles related to hydrogen bond, see also Fig. 56A-1-005, Fig. 56A-1-006.			
4	Thermal expansion: Fig. 56A-1-007, Fig. 56A-1-008.			
5a	Dielectric constant: Fig. 56A-1-009, Fig. 56A-1-010, Fig. 56A-1-011.			
	Dielectric dispersion: Fig. 56A-1-012, Fig. 56A-1-013, Fig. 56A-1-014, Fig. 56A-1-015.			
c, d	Spontaneous polarization and pyroelectric coefficient: Fig. 56A-1-016.			
6a	Heat capacity: see			92Min
9a	Birefringence: Fig. 56A-1-017.			
	Infrared spectra: see			88Jak, 92Var
10a	Raman scattering: see			91Min, 92Var
13a	NMR: Fig. 56A-1-018.			

Table 56A-1-001. $[(CH_3)_2NH_2]_3Sb_2Cl_9$. Crystal structure of phase I [88Gda]. Fractional coordinates and equivalent isotropic temperature parameters. The isotropic temperature parameter U_{eq} is defined as $U_{eq} = (U_{11} \cdot U_{22} \cdot U_{33})^{1/3}$, U_{ij} is defined by Eq. (d) in Introduction. $T = 293$ K. One kind of cations shown by N(2) and C(3) is disordered with two configurations. See Fig. 56A-1-003.

Atom	*x*	*y*	*z*	U_{eq} [Å^2]
Sb(1)	0.16395(3)	0.03898(5)	0.33933(4)	0.0555(2)
Cl(1)	0.3027(2)	0.0838(3)	0.2090(2)	0.0859(8)
Cl(2)	0.0668(2)	0.2201(2)	0.2086(2)	0.0914(8)
Cl(3)	0.2227(2)	0.2755(3)	0.5172(2)	0.0960(9)
Cl(4)	0.1066(2)	–0.1464(2)	0.1589(2)	0.0902(8)
Cl(5)	0.0	0.0	0.5	0.139(2)
N(1)	–0.136(1)	–0.070(2)	0.167(2)	0.21(1)
C(1)	–0.145(1)	–0.206(1)	0.121(1)	0.131(5)
C(2)	–0.220(2)	0.025(2)	0.191(2)	0.167(8)
N(2)	0.491(2)	0.064(2)	0.468(3)	0.125(9)
C(3)	0.4664(9)	0.075(1)	0.594(1)	0.114(5)

Table 56A-1-002. $[(CH_3)_2NH_2]_3Sb_2Cl_9$. Anisotropic temperature parameters in phase I [88Gda]. U_{ij} [Å^2] is defined by Eq. (d) in Introduction. $T = 293$ K.

Atom	U_{11}	U_{22}	U_{33}	U_{12}	U_{13}	U_{23}
Sb(1)	0.0520(4)	0.0540(3)	0.0609(3)	0.0003(2)	0.0083(2)	0.0012(2)
Cl(1)	0.069(1)	0.096(1)	0.095(1)	–0.006(1)	0.028(1)	0.003(1)
Cl(2)	0.096(2)	0.087(1)	0.092(1)	0.026(1)	–0.005(1)	0.013(1)
Cl(3)	0.102(2)	0.101(2)	0.086(1)	–0.019(1)	0.001(1)	–0.005(1)
Cl(4)	0.091(2)	0.080(1)	0.101(1)	–0.013(1)	0.003(1)	–0.021(1)
Cl(5)	0.098(4)	0.141(3)	0.196(5)	–0.019(3)	0.050(3)	0.009(3)
N(1)	0.14(1)	0.19(2)	0.33(3)	–0.00(1)	–0.03(1)	–0.07(2)
C(1)	0.15(1)	0.114(9)	0.133(8)	–0.021(9)	0.037(8)	–0.020(8)
C(2)	0.31(3)	0.11(1)	0.13(1)	0.08(1)	0.08(1)	0.002(8)
N(2)	0.11(2)	0.10(1)	0.18(2)	0.02(1)	0.02(2)	0.03(1)
C(3)	0.109(9)	0.102(7)	0.133(9)	–0.008(6)	0.033(7)	–0.026(7)

Table 56A-1-003. $[(CH_3)_2NH_2]_3Sb_2Cl_9$. Crystal structure of phase I [96Zal]. Fractional coordinates and equivalent isotropic temperature parameters. The isotropic temperature parameter U_{eq} [Å^2] is defined as $U_{eq} = (1/3)\Sigma U_{ij}\, a_i^*\, a_j^*\, \boldsymbol{a}_i \cdot \boldsymbol{a}_j$. U_{ij} is defined by Eq. (d) in Introduction. $T = 298$ K. In this model two kinds of crystallographically non-equivalent cations are disordered. The cations composed of N(1), C(11) and C(12) have two configurations, while other ones have three. Three configurations are composed of {N(21), C(2), C(31)}, {N(22), C(2), C(31)} and {N(23), C(2), C(32)}, respectively.

Atom	*x*	*y*	*z*	U_{eq}
Sb(1)	0.1640(1)	0.0391(1)	0.3394(1)	0.048(1)
Cl(1)	0.0670(1)	0.2206(2)	0.2094(2)	0.085(1)
Cl(2)	0.3028(1)	0.0841(2)	0.2094(2)	0.079(1)
Cl(3)	0.1062(1)	–0.1467(2)	0.1591(2)	0.083(1)
Cl(4)	0.2235(1)	0.2755(2)	0.5170(2)	0.090(1)
Cl(5)	0.0	0.0	1/2	0.132(1)
N(1)	0.4973(9)	0.0627(10)	0.4613(9)	0.121(1)
C(11)	0.5367(10)	–0.0824(11)	0.4352(11)	0.106(1)
C(12)	0.4706(10)	0.0714(11)	0.6032(10)	0.098(1)
N(21)	0.3675(7)	0.5510(10)	0.1419(10)	0.095(1)
N(22)	0.3572(9)	0.5976(11)	0.2207(10)	0.095(1)
N(23)	0.2818(12)	0.6183(13)	0.1470(13)	0.081(1)
C(2)	0.3548(5)	0.7005(8)	0.1256(7)	0.119(1)
C(31)	0.2913(7)	0.4693(9)	0.1900(8)	0.133(1)
C(32)	0.2210(13)	0.4916(13)	0.1792(13)	0.109(1)

Table 56A-1-004. $[(CH_3)_2NH_2]_3Sb_2Cl_9$. Crystal structure of phase II [96Zal]. Fractional coordinates and equivalent isotropic temperature parameters. The isotropic temperature parameter U_{eq} [Å^2] is defined as $U_{eq} = (1/3)\Sigma U_{ij}\, a_i^*\, a_j^*\, \boldsymbol{a}_i \cdot \boldsymbol{a}_j$. U_{ij} is defined by Eq. (d) in Introduction. T = 200 K. Atom numbering scheme of Sb and Cl atoms are different from those in [88Gda]. One of the three crystallographically non-equivalent cations is disordered. The disorder is realized by splitting the N and C atoms between two positions with occupancy factors 0.73 for N(31), C(51) and C(61), and 0.27 for N(32), C(52) and C(62).

Atom	x	y	z	U_{eq}
Sb(1)	0.0	0.2102	0.0	0.026(1)
Sb(2)	0.1687(1)	0.7043(1)	0.3245(1)	0.025(1)
Cl(1)	0.2758(1)	0.5329(2)	0.4541(2)	0.041(1)
Cl(2)	–0.0809(2)	0.0217(2)	–0.1457(2)	0.048(1)
Cl(3)	–0.0523(2)	0.3923(2)	–0.1830(2)	0.041(1)
Cl(4)	0.0490(1)	–0.0347(2)	0.1925(2)	0.045(1)
Cl(5)	0.0363(1)	0.6554(2)	0.4571(2)	0.041(1)
Cl(6)	0.1514(1)	0.1663(2)	–0.1279(2)	0.042(1)
Cl(7)	0.2224(2)	0.8972(2)	0.5227(2)	0.043(1)
Cl(8)	0.1083(1)	0.4853(2)	0.1564(2)	0.044(1)
Cl(9)	0.3338(1)	0.7617(2)	0.1149(2)	0.055(1)
N(1)	–0.1609(4)	–0.1801(5)	0.1172(5)	0.049(1)
C(1)	–0.2039(6)	–0.1668(8)	0.2497(7)	0.056(1)
C(2)	–0.1333(6)	–0.3313(8)	0.0837(9)	0.072(1)
N(2)	0.2070(4)	0.6972(5)	–0.1883(5)	0.046(1)
C(3)	0.1969(4)	0.5350(6)	–0.2025(6)	0.041(1)
C(4)	0.1177(6)	0.7667(7)	–0.1548(6)	0.063(1)
N(31)	0.5518(5)	0.8724(7)	0.5331(7)	0.046(1)
C(51)	0.6001(9)	0.7371(9)	0.4941(9)	0.085(1)
C(61)	0.4495(6)	0.8875(11)	0.5023(8)	0.074(1)
N(32)	0.4715(12)	0.8178(13)	0.4844(13)	0.093(1)
C(52)	0.5392(12)	0.7150(13)	0.4512(13)	0.086(1)
C(62)	0.4959(13)	0.9734(13)	0.5430(14)	0.102(1)

Table 56A-1-005. $[(CH_3)_2NH_2]_3Sb_2Cl_9$. Crystal structure of phase I [88Gda]. Bond distances [Å] and angles [°]. $T = 293$ K.

Bond distances [Å]			
Sb(1)–Cl(1)	2.453(2)	N(1)–C(1)	1.31(2)
Sb(1)–Cl(2)	2.408(2)	N(1)–C(2)	1.49(2)
Sb(1)–Cl(3)	2.814(2)	N(2)–C(3)	1.30(3)
Sb(1)–Cl(4)	2.494(2)	N(2)–C(3^{ii})	1.54(3)
Sb(1)–Cl(5)	2.919(1)		
Sb(1)–Cl(3^{i})	3.111(2)		
Angles [°]			
Cl(1)–Sb(1)–Cl(2)	93.2(1)	Cl(3)–Sb(1)–Cl(4)	172.8(1)
Cl(1)–Sb(1)–Cl(3)	89.3(1)	Cl(3)–Sb(1)–Cl(5)	88.1(1)
Cl(1)–Sb(1)–Cl(4)	88.3(1)	Cl(3)–Sb(1)–Cl(3^{i})	101.5(1)
Cl(1)–Sb(1)–Cl(5)	177.2(1)	Cl(4)–Sb(1)–Cl(5)	94.2(1)
Cl(1)–Sb(1)–Cl(3^{i})	87.6(1)	Cl(4)–Sb(1)–Cl(3^{i})	85.3(1)
Cl(2)–Sb(1)–Cl(3)	85.7(1)	Cl(5)–Sb(1)–Cl(3^{i})	93.8(1)
Cl(2)–Sb(1)–Cl(4)	87.6(1)	C(1)–N(1)–C(2)	122(2)
Cl(2)–Sb(1)–Cl(5)	85.7(1)	C(3)–N(2)–C(3^{ii})	125(2)
Cl(2)–Sb(1)–Cl(3^{i})	172.8(1)	Sb(1)–Cl(3^{i})–Sb(1^{ii})	163.6(1)

Symmetry codes: (i) $0.5 - x$, $-0.5 + y$, $1 - z$;
(ii) $0.5 - x$, $0.5 + y$, $1 - z$.

Table 56A-1-006. $[(CH_3)_2NH_2]_3Sb_2Cl_9$. Crystal structure of phase II [96Zal]. Bond distances [Å] and angles [°]. $T = 200$ K.

Bond distances [Å]			
Sb(1)–Cl(2)	2.405(2)	Sb(2)–Cl(9)	3.247(2)
Sb(1)–Cl(3)	2.447(2)	N(1)–C(1)	1.45(1)
Sb(1)–Cl(4)	2.905(2)	N(1)–C(2)	1.46(1)
Sb(1)–Cl(6)	2.587(2)	N(2)–C(3)	1.48(1)
Sb(1)–Cl(8)	3.199(2)	N(2)–C(4)	1.47(1)
Sb(2)–Cl(1)	2.409(2)	N(31)–C(51)	1.46(1)
Sb(2)–Cl(5)	2.393(2)	N(31)–C(61)	1.45(1)
Sb(2)–Cl(7)	2.617(2)	N(32)–C(52)	1.39(2)
Sb(2)–Cl(8)	2.625(2)	N(32)–C(62)	1.54(2)
Angles [°]			
Cl(2)–Sb(1)–Cl(3)	88.8(1)	Cl(1)–Sb(2)–Cl(9)	87.9(1)
Cl(2)–Sb(1)–Cl(4)	83.7(1)	Cl(5)–Sb(2)–Cl(7)	86.0(1)
Cl(2)–Sb(1)–Cl(6)	89.3(1)	Cl(5)–Sb(2)–Cl(8)	87.6(1)
Cl(2)–Sb(1)–Cl(8)	172.5(1)	Cl(5)–Sb(2)–Cl(9)	174.0(1)
Cl(3)–Sb(1)–Cl(4)	172.5(1)	Cl(7)–Sb(2)–Cl(8)	171.4(1)
Cl(3)–Sb(1)–Cl(6)	88.6(1)	Cl(7)–Sb(2)–Cl(9)	99.2(1)
Cl(3)–Sb(1)–Cl(8)	84.3(1)	Cl(8)–Sb(2)–Cl(9)	87.6(1)
Cl(4)–Sb(1)–Cl(6)	91.2(1)	Sb(1)–Cl(8)–Sb(2)	167.3(1)
Cl(4)–Sb(1)–Cl(8)	103.2(1)	C(1)–N(1)–C(2)	114(1)
Cl(6)–Sb(1)–Cl(8)	87.7(1)	C(3)–N(2)–C(4)	112(1)
Cl(1)–Sb(2)–Cl(5)	95.5(1)	C(51)–N(31)–C(61)	121(1)
Cl(1)–Sb(2)–Cl(7)	86.6(1)	C(52)–N(32)–C(62)	124(2)
Cl(1)–Sb(2)–Cl(8)	88.4(1)		

Table 56A-1-007. $[(CH_3)_2NH_2]_3Sb_2Cl_9$. Crystal structure [96Zal]. Bond distances [Å] and angles [°] related to hydrogen bond. T = 200 and 298 K. For atom numbering scheme see [96Zal], and for the fractional coordinates at 298 K see Table 56A-1-003.

D–H…*A*	*D*...H	H–*A*	*D*…*A*	*D*–H...*A*
T = 200 K				
N(1)–H(1*A*)...Cl(6^{i})	0.98(3)	2.46(4)	3.34(1)	150(3)
N(1)–H(1*B*)...Cl(4)	0.82(3)	2.45(4)	3.25(1)	162(3)
N(2)–H(2*A*)...Cl(9)	0.92(3)	2.39(3)	3.28(1)	163(3)
N(2)–H(2*B*)...Cl(7^{ii})	0.91(3)	2.40(4)	3.30(1)	171(3)
N(31)–H(31*A*)...Cl(6^{iii})	0.97(3)	2.47(3)	3.39(1)	157(3)
N(31)–H(31*B*)...Cl(7^{iv})	0.82(3)	2.47(3)	3.18(1)	146(3)
T = 298 K				
N(1)–H(1*A*)...Cl(2)	0.90	2.63	3.49(1)	162(3)
N(1)–H(1*B*)...Cl(4^{v})	0.90	2.66	3.48(1)	151(3)
(N21)–H(21*A*)...Cl(3^{vi})	0.90	2.58	3.46(2)	168(3)
N(22)–H(22*B*)...Cl(4^{vii})	0.90	2.41	3.29(1)	167(3)
N(23)–H(23*A*)...Cl(4^{vii})	0.90	2.69	3.56(1)	161(3)

Symmetry codes: (i) $x, -y, z - 1/2$;
(ii) $x - 1, y, z$;
(iii) $x + 1, 1 - y, z + 1/2$;
(iv) $x, 2 - y, z + 1/2$;
(v) $x, 1/2 - y, 1/2 + z$;
(vi) $-x, 1/2 + y, 1/2 - z$;
(vii) $1 - x, 1/2 + y, 1/2 - z$.

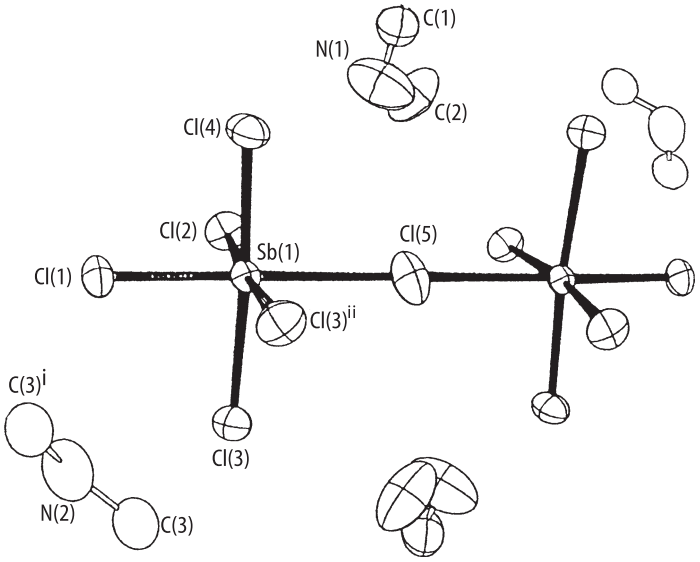

Fig. 56A-1-001. $[(CH_3)_2NH_2]_3Sb_2Cl_9$. Fragment of the structure, showing the atom numbering scheme, Sb coordination and positions of $(CH_3)_2NH_2^+$ cations [88Gda]. $T = 293$ K. i, ii: symmetry codes, see Table 56A-1-005.

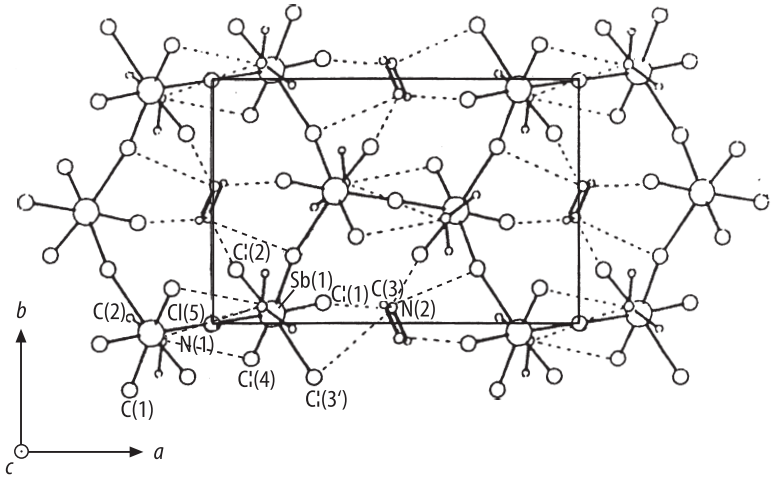

Fig. 56A-1-002. $[(CH_3)_2NH_2]_3Sb_2Cl_9$. Structure [88Gda]. Projection along the *c* axis showing the two-dimensional network of $(Sb_2Cl_9^{-3})_n$ polyanions. $T = 293$ K.

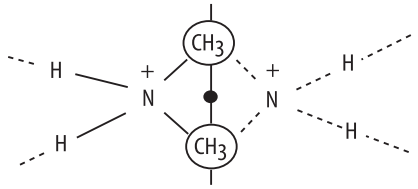

Fig. 56A-1-003. $[(CH_3)_2NH_2]_3Sb_2Cl_9$. Structure [88Gda]. Two equivalent positions of dimethylammonium cations in the paraelectric phase. Two configurations are related to each other by a 180° rotation around the axis passing through the methyl groups, the midpoint of which corresponds to the center of inversion.

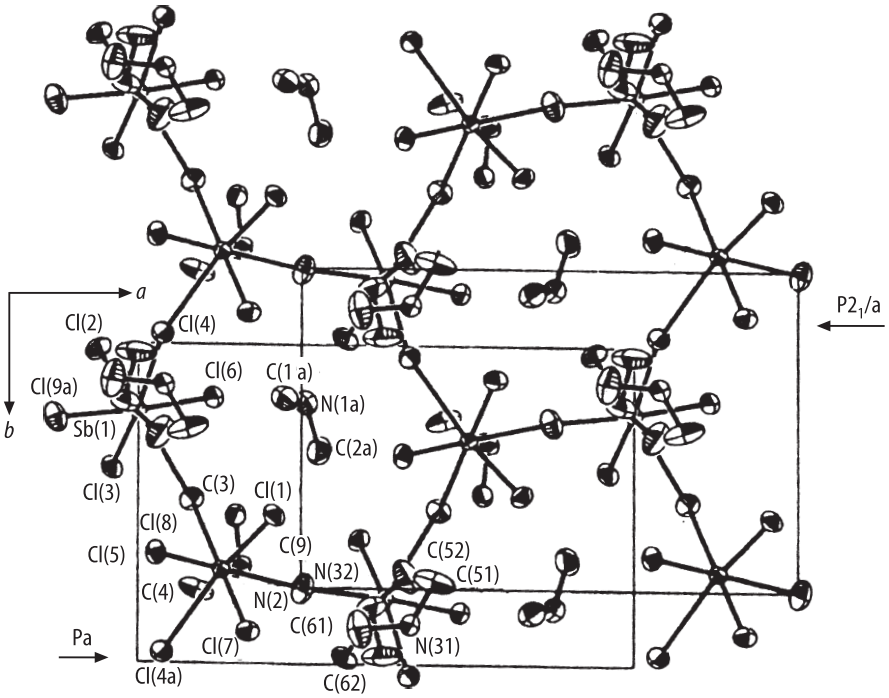

Fig. 56A-1-004. $[(CH_3)_2NH_2]_3Sb_2Cl_9$. Structure [96Zal]. Projection along the *c* axis viewed from the negative direction. $T = 200$ K. The choice of the unit cell in phase I and II is shown.

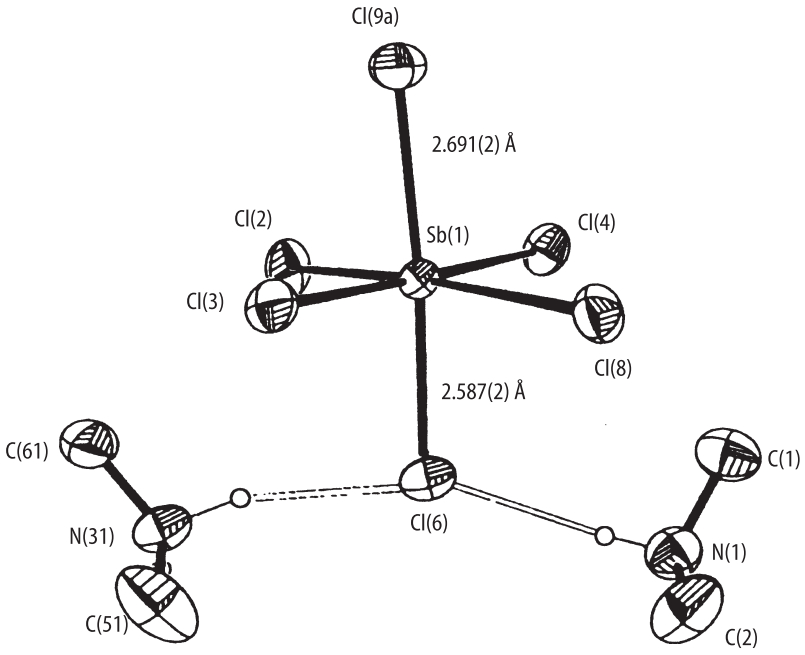

Fig. 56A-1-005. $[(CH_3)_2NH_2]_3Sb_2Cl_9$. Structure [96Zal]. Scheme of hydrogen bonding involving Cl(6) atom, resulting in elongation of the Sb(1)–Cl(6) bond from a mean value of 2.45 Å to 2.587 Å. $T = 200$ K.

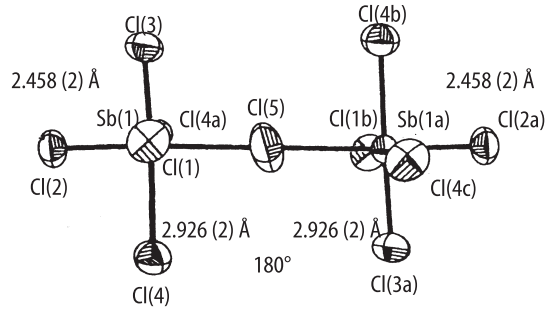

a

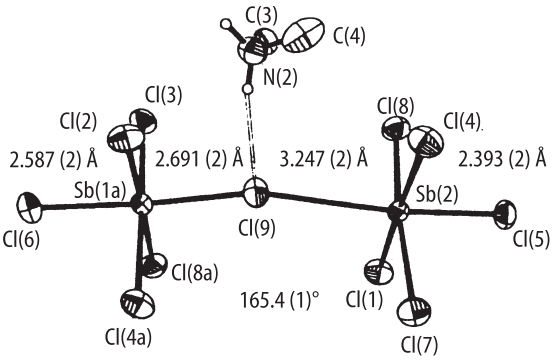

b

Fig. 56A-1-006. $[(CH_3)_2NH_2]_3Sb_2Cl_9$. Structure [96Zal]. Scheme of hydrogen bonding involving the bridging atom Cl(5) atom at (**a**) 298 K and (**b**) 200 K. A different numbering scheme is used at 200 and 298 K, but atoms are the same. At T = 200 K N(2)–H(2A)---Cl(9) indicate hydrogen bond.

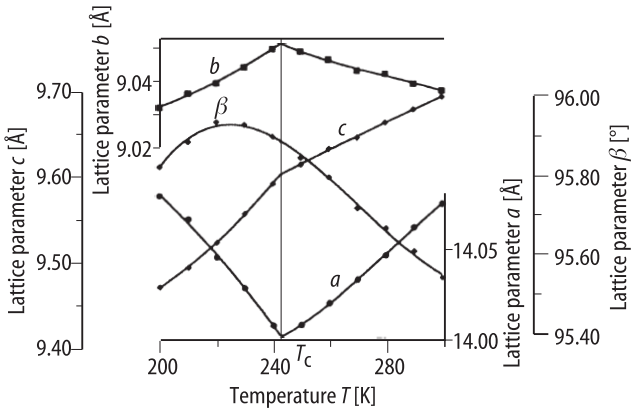

Fig. 56A-1-007. $[(CH_3)_2NH_2]_3Sb_2Cl_9$. a, b, c, β vs. T [96Zal]. a, b, c, β: lattice parameters.

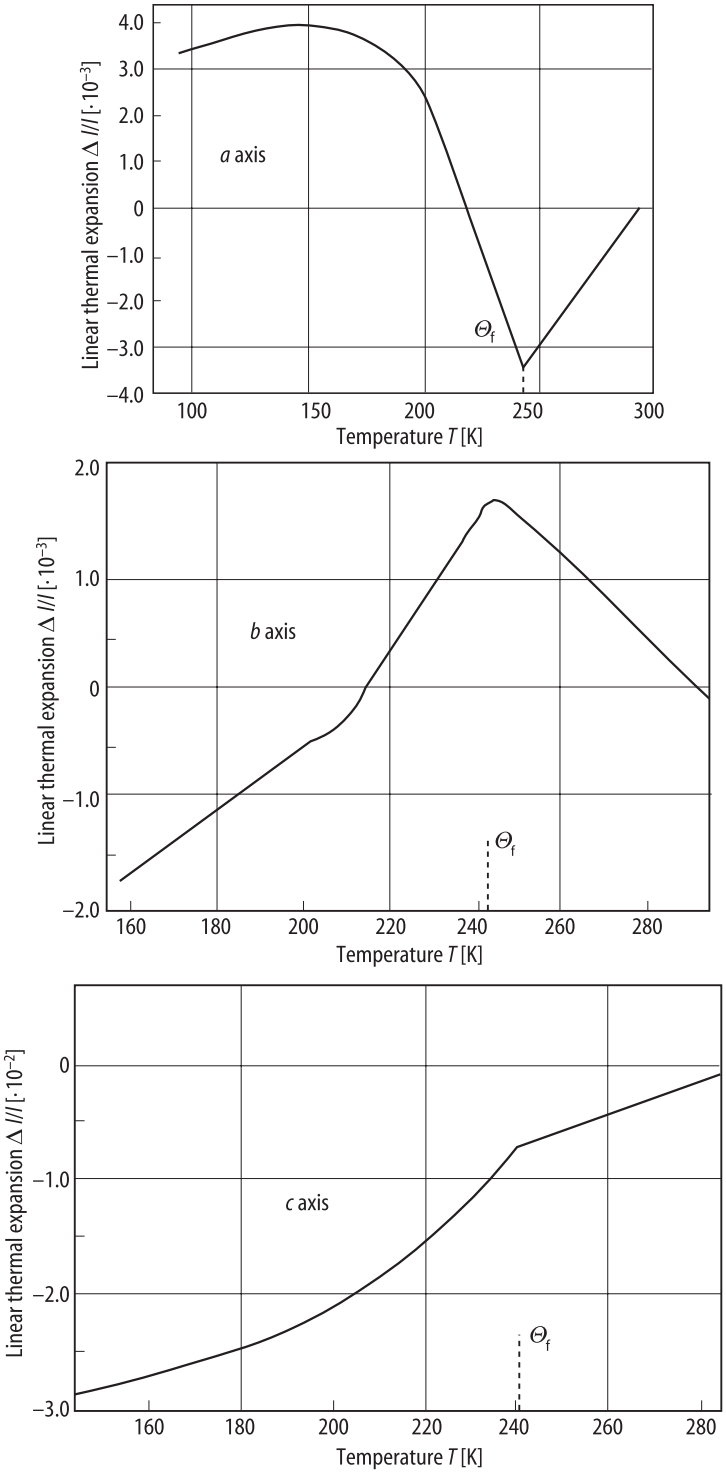

Fig. 56A-1-008. $[(CH_3)_2NH_2]_3Sb_2Cl_9$. $\Delta l/l$ vs. T [95Jak]. $\Delta l/l$: linear thermal expansion along the a, b and c axes.

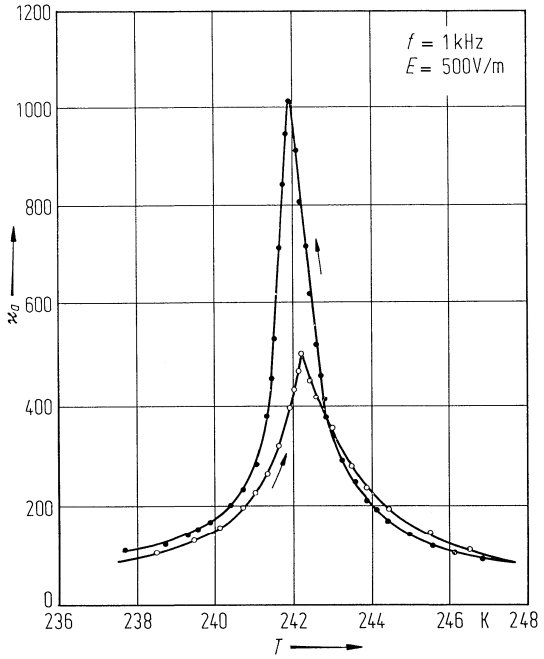

Fig. 56A-1-009. $[(CH_3)_2NH_2]_3Sb_2Cl_9$. κ_a vs. T [86Jak].

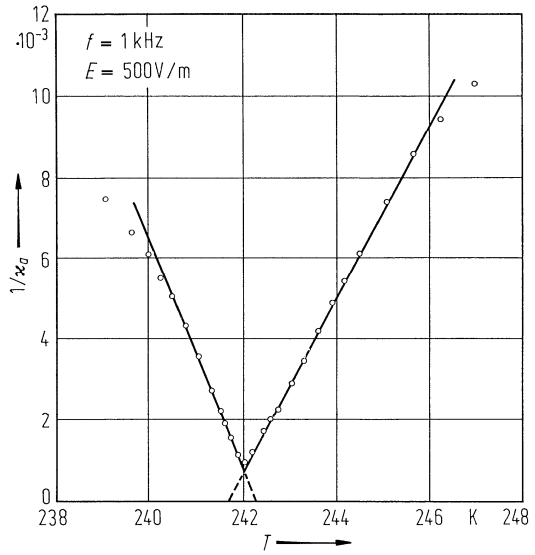

Fig. 56A-1-010. $[(CH_3)_2NH_2]_3Sb_2Cl_9$. $1/\kappa_a$ vs. T [86Jak].

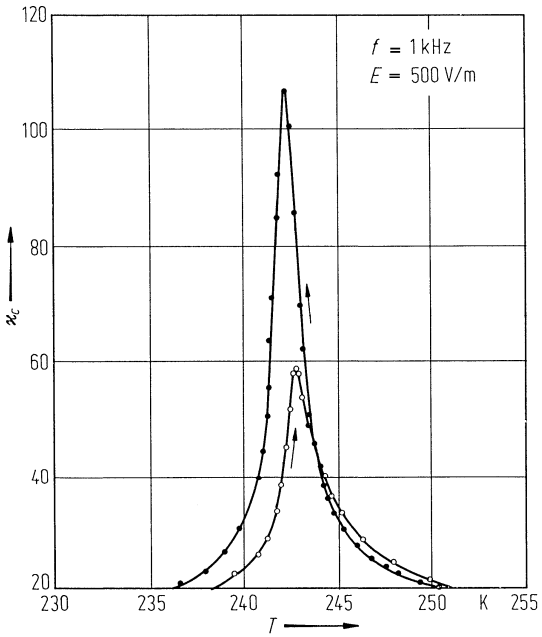

Fig. 56A-1-011. $[(CH_3)_2NH_2]_3Sb_2Cl_9$. κ_c vs. T [86Jak].

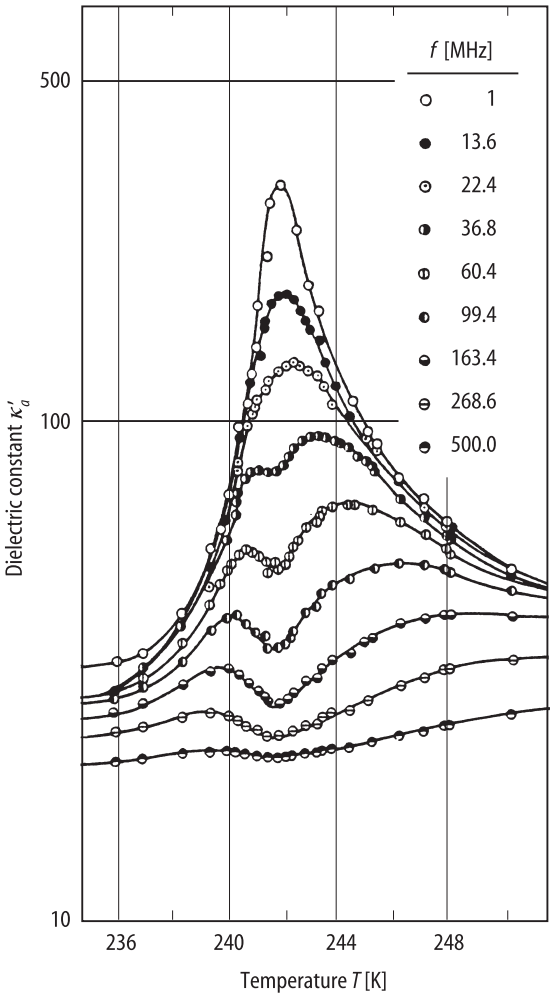

Fig. 56A-1-012. $[(CH_3)_2NH_2]_3Sb_2Cl_9$. κ_a' vs. T [95Bat]. Parameter: f.

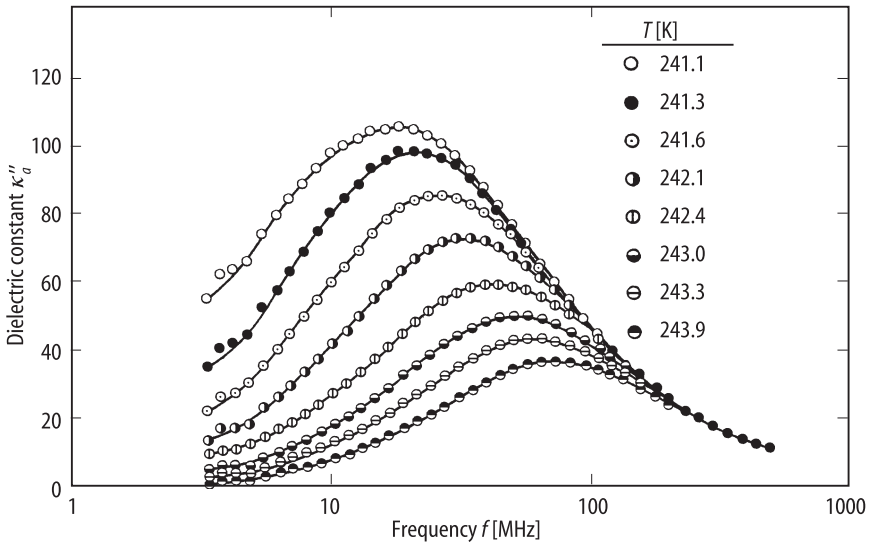

Fig. 56A-1-013. $[(CH_3)_2NH_2]_3Sb_2Cl_9$. κ_a'' vs. f [95Bat]. Parameter: T.

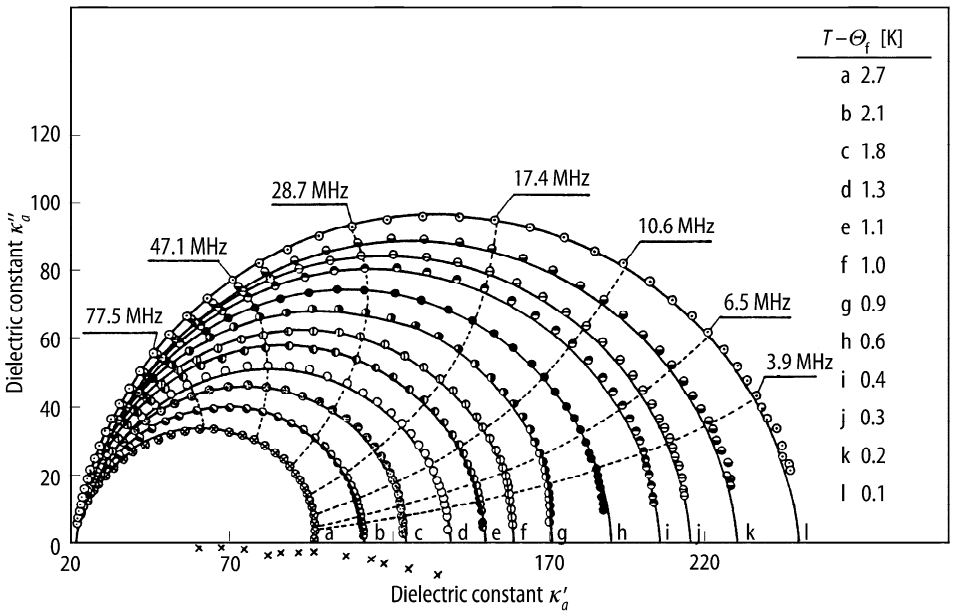

Fig. 56A-1-014. $[(CH_3)_2NH_2]_3Sb_2Cl_9$. Cole-Cole plot of complex dielectric constant [95Bat].

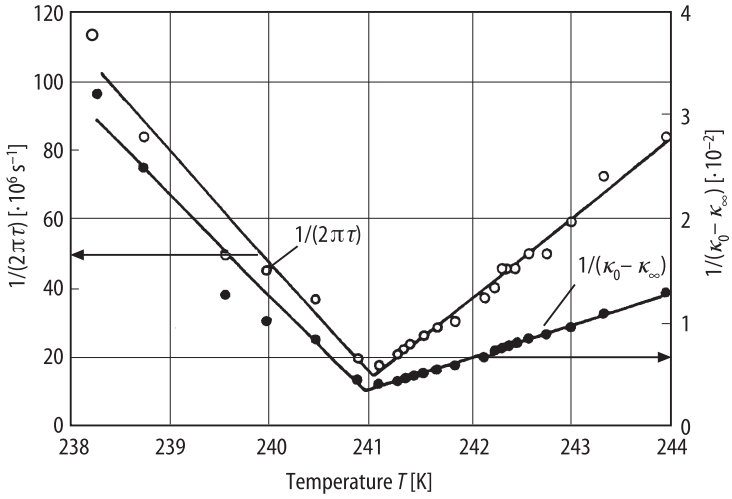

Fig. 56A-1-015. $[(CH_3)_2NH_2]_3Sb_2Cl_9$. $1/(2\pi\tau)$, $1/(\kappa_0-\kappa_\infty)$ vs. T [95Bat]. τ: dielectric relaxation time, κ_0, κ_∞: static and high frequency dielectric constant.

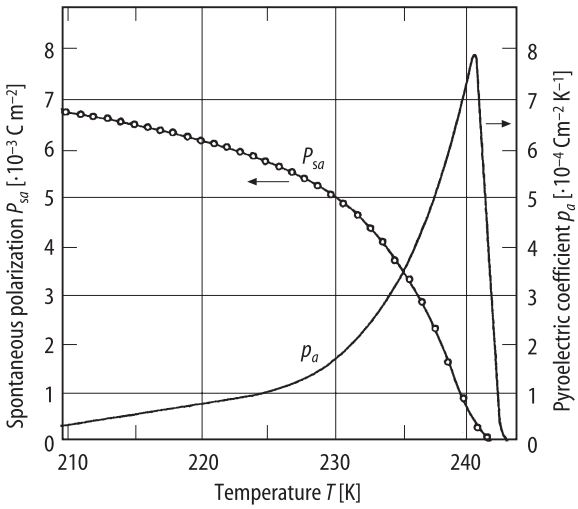

Fig. 56A-1-016. $[(CH_3)_2NH_2]_3Sb_2Cl_9$. p_a, P_{sa} vs. T [87Min]. p_a, P_{sa}: pyroelectric coefficient, spontaneous polarization along the a axis.

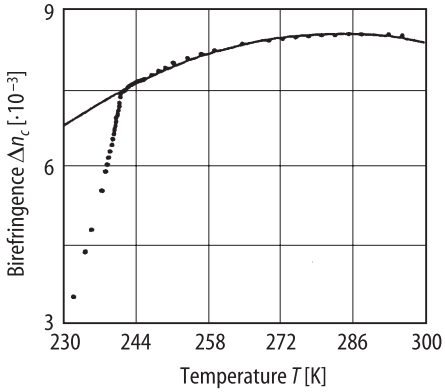

Fig. 56A-1-017. $[(CH_3)_2NH_2]_3Sb_2Cl_9$. Δn_c vs. T [92Prz]. Δn_c: birefringence measured along [001]. λ = 632.8 nm.

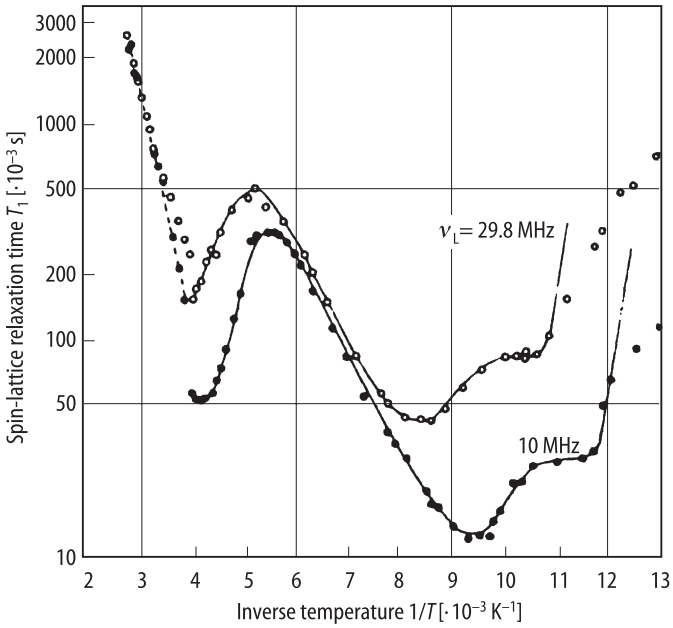

Fig. 56A-1-018. $[(CH_3)_2NH_2]_3Sb_2Cl_9$. T_1 vs. $1/T$ [94Jag]. T_1: proton spin-lattice relaxation time in powder. Open circle: ν_L = 29.8 MHz, full circle: ν_L = 10 MHz.

References

86Jak Jakubas, R.: Solid State Commun. **60** (1986) 389.
87Min Miniewicz, A., Jakubas, R.: Solid State Commun. **63** (1987) 933.
88Gda Gdaniec, M., Kosturkiewicz, Z., Jakubas, R., Sobczyk, L.: Ferroelectrics **77** (1988) 31.
88Jak Jakubas, R., Malarski, Z., Sobczyk, L.: Ferroelectrics **80** (1988) 193.
91Min Miniewicz, A., Lefebvre, J., Jakubas, R.: J. Raman Spectrosc. **22** (1991) 435.
92Min Miniewicz, A., Sworakowski, J., Bertault, M., Jakubas, R.: Ferroelectrics **125** (1992) 39.
92Prz Przesławski, J., Kosturek, B., Jakubas, R.: Ferroelectrics **126** (1992) 91.
92Var Varma, V., Bhattaacharjee, R., Vasan, H.N., Rao, C.N.R.: Spectrochim. Acta A **48** (1992) 1631.
94Jag Jagadeesh, B., Rajan, K., Venu, K., Sastry, V.S.S.: Solid State Commun. **91** (1994) 843.
95Bat Bator, G., Jakubas, R.: Phys. Status Solidi (a) **147** (1995) 591.
95Jak Jakubas, R., Mróz, J., François, P., Lefebvre, J.: Ferroelectrics **173** (1995) 221.
96Zal Zaleski, J., Pietraszko, A.: Acta Crystallogr. Sect. B **52** (1996) 287.

No. 56A-2 $[(CH_3)_3NH]_3Sb_2Cl_9$, Trimethylammonium nonachlorodiantimonate

(M = 742.93)

1a Ferroelectric activity in $[(CH_3)_3NH]_3Sb_2Cl_9$ was discovered by Jakubas in 1986. 86Jak1

b

phase	V	IV	III	II	I
state	F [b])	F [b])	F [a])		P [a])
crystal system			monoclinic		
space group			Pc – C_s^{2} [c])		
Θ [K]		127 [e])[f])	203 [e])	363 [d])	364 [d])

[a]) 86Jak1
[b]) 86Jak2
[c]) 85Kal
[d]) 89Min1
[e]) 93Bat
[f]) 87Idz

P_s || [001]. Additional small component of P_s was observed along the b axis in phases IV and V; see 93Bat
Transparent, colorless. Cleavage plane perpendicular to the a axis. 86Mro
Decomposition at about 415 K. 95Tom
$\rho_X = 1.744(2) \cdot 10^3$ kg m^{-3}. 85Kal

2a Crystal growth: slow evaporation of aqueous solution of $[(CH_3)_3NH]Cl$ and $SbCl_3$ at the stoichiometric molar ratio. 85Kal

3a Unit cell parameters: a = 10.085(3) Å, b = 9.072(4) Å, c = 15.459(6) Å, β = 90.17(3)° at 296 K. 85Kal

b Z = 2 in phase III. 85Kal
Crystal structure: Fig. 56A-2-001, Fig. 56A-2-002.
Positional and temperature parameters: Table 56A-2-001.
Interatomic distances and bond angles: Table 56A-2-002.

4 Thermal expansion: Fig. 56A-2-003.

5a Dielectric constant: Fig. 56A-2-004, Fig. 56A-2-005, Fig. 56A-2-006, Fig. 56A-2-007.
Dielectric dispersion: Fig. 56A-2-008, Fig. 56A-2-009, Fig. 56A-2-010, Fig. 56A-2-011.

c Spontaneous polarization: Fig. 56A-2-012, Fig. 56A-2-013, Fig. 56A-2-014.

6a Heat capacity: see 89Jak

9a Birefringence: see 92Prz
Infrared transmission: see 92Var

10a Raman scattering: Fig. 56A-2-015, Fig. 56A-2-016, Fig. 56A-2-017, Fig. 56A-2-018, Fig. 56A-2-019.

b Brillouin scattering: Fig. 56A-2-020.

13a NMR: Fig. 56A-2-021, Fig. 56A-2-022.

14b Quasi-elastic neutron scattering: see 92Urb

15b Domain switching: Fig. 56A-2-023.

Table 56A-2-001. $[(CH_3)_3NH]_3Sb_2Cl_9$. Crystal structure of phase III [85Kal]. Fractional coordinates and equivalent isotropic temperature parameters. The isotropic temperature parameter U_{eq} is defined as $U_{eq} = (U_{11} + U_{22} + U_{33})/3$, U_{ij} is defined by Eq. (d) in Introduction. $T = 296$ K.

Atom	*x*	*y*	*z*	U_{eq} [Å^2]
Sb(1)	0.0	0.21025(6)	0.0	0.0452(4)
Sb(2)	0.30281(5)	0.71061(6)	0.17241(3)	0.0433(4)
Cl(1)	0.4202(3)	0.5155(3)	0.2456(2)	0.063(1)
Cl(2)	–0.1191(3)	0.0385(3)	–0.0892(2)	0.065(2)
Cl(3)	–0.1274(3)	0.4131(3)	–0.0638(2)	0.070(2)
Cl(4)	0.1518(3)	–0.0526(3)	0.0570(2)	0.087(2)
Cl(5)	0.4266(3)	0.6605(3)	0.0424(2)	0.062(1)
Cl(6)	–0.1700(3)	0.1766(3)	0.1118(2)	0.067(2)
Cl(7)	0.4774(2)	0.8882(3)	0.2146(2)	0.065(1)
Cl(8)	0.1196(3)	0.4841(3)	0.1190(2)	0.069(2)
Cl(9)	0.1862(2)	0.7738(3)	0.3591(2)	0.074(2)
N(1)	–0.1482(8)	0.6728(9)	0.1431(6)	0.066(5)
N(2)	0.4489(8)	0.8069(9)	0.4802(8)	0.080(6)
N(3)	0.1508(11)	–0.1971(11)	–0.1498(7)	0.101(9)
C(11)	–0.242(1)	0.564(1)	0.1787(11)	0.100(9)
C(12)	–0.114(1)	0.779(2)	0.2097(7)	0.100(9)
O(13)	–0.205(1)	0.746(1)	0.0653(7)	0.089(8)
O(21)	0.511(1)	0.961(1)	0.4778(10)	0.098(9)
C(22)	0.534(1)	0.695(1)	0.4372(7)	0.093(8)
C(23)	0.422(1)	0.759(1)	0.5720(9)	0.104(9)
C(31)	0.129(2)	–0.344(2)	–0.1139(11)	0.15(1)
C(32)	0.296(2)	–0.183(1)	–0.1666(12)	0.13(1)
C(33)	0.088(3)	–0.160(3)	–0.2334(13)	0.25(2)
H(1) *)	–0.070	0.624	0.125	0.10
H(2)	0.368	0.813	0.449	0.10
H(3)	0.112	–0.134	–0.108	1.11

*) Atoms not refined.

Table 56A-2-002. $[(CH_3)_3NH]_3Sb_2Cl_9$. Crystal structure of phase III [85Kal]. Bond distances [Å] and angles [°].

Interatomic distances [Å]			
Sb(1)–Cl(2)	2.401(3)	Sb(2)–Cl(1)	2.410(3)
Sb(1)–Cl(3)	2.450(3)	Sb(2)–Cl(5)	2.412(3)
Sb(1)–Cl(6)	2.457(3)	Sb(2)–Cl(7)	2.473(3)
Sb(1)–Cl(4)	2.966(3)	Sb(2)–Cl(8)	2.883(3)
Sb(1)–Cl(8)	3.316(3)	Sb(2)–Cl(9)	3.172(3)
Sb(1)–Cl(9) [i])	2.884(3)	Sb(2)–Cl(4) [ii])	3.178(3)

Bond angles [°]			
Cl(2)–Sb(1)–Cl(3)	89.74(9)	Cl(1)–Sb(2)–Cl(5)	89.90(9)
Cl(2)–Sb(1)–Cl(6)	88.53(10)	Cl(1)–Sb(2)–Cl(7)	90.35(9)
Cl(2)–Sb(1)–Cl(4)	84.59(10)	Cl(1)–Sb(2)–Cl(8)	85.69(9)
Cl(2)–Sb(1)–Cl(8)	170.21(8)	Cl(1)–Sb(2)–Cl(9)	83.61(8)
Cl(2)–Sb(1)–Cl(9) [i])	85.67(8)	Cl(1)–Sb(2)–Cl(4) [ii])	173.71(9)
Cl(3)–Sb(1)–Cl(6)	90.60(9)	Cl(5)–Sb(2)–Cl(7)	88.44(9)
Cl(3)–Sb(1)–Cl(4)	173.22(9)	Cl(5)–Sb(2)–Cl(8)	87.70(9)
Cl(3)–Sb(1)–Cl(8)	81.36(9)	Cl(5)–Sb(2)–Cl(9)	170.52(8)
Cl(3)–Sb(1)–Cl(9) [i])	90.00(8)	Cl(5)–Sb(2)–Cl(4) [ii])	84.70(9)
Cl(6)–Sb(1)–Cl(4)	92.97(10)	Cl(7)–Sb(2)–Cl(8)	174.47(8)
Cl(6)–Sb(1)–Cl(8)	87.50(8)	Cl(7)–Sb(2)–Cl(9)	84.72(8)
Cl(6)–Sb(1)–Cl(9) [i])	174.16(8)	Cl(7)–Sb(2)–Cl(4) [ii])	92.71(9)
Cl(4)–Sb(1)–Cl(8)	104.54(8)	Cl(8)–Sb(2)–Cl(9)	98.65(8)
Cl(4)–Sb(1)–Cl(9) [i])	85.87(8)	Cl(8)–Sb(2)–Cl(4) [ii])	90.87(9)
Cl(8)–Sb(1)–Cl(9) [i])	98.33(7)	Cl(9)–Sb(2)–Cl(4) [ii])	102.14(8)
		Sb(1)–Cl(4)–Sb(2) [iii])	162.96(12)
		Sb(1)–Cl(8)–Sb(2)	157.62(10)
		Sb(1) [iv])–Cl(9)–Sb(2)	160.13(9)

Hydrogen bonding N–H···Cl	N–H [Å]	H···Cl	N···Cl	N–H–Cl [°]
N(1)–H(1)···Cl(8)	0.95	2.29	3.220(9)	165
N(2)–H(2)···Cl(9)	0.95	2.33	3.254(10)	166
N(3)–H(3)···Cl(4)	0.95	2.69	3.455(11)	139
N(3)–H(3)···Cl(2)	0.95	2.82	3.588(11)	138

Symmetry code: (i) x, $1 - y$, $z - 1/2$; (ii) x, $1 + y$, z;
(iii) x, $y - 1$, z; (iv) x, $1 - y$, $z + 1/2$.

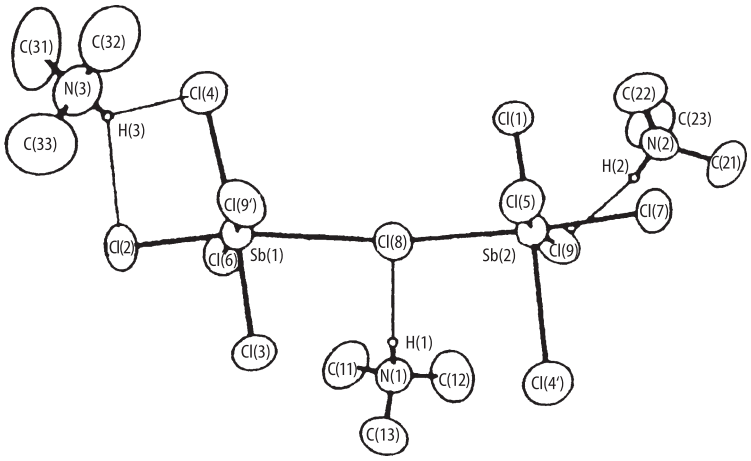

Fig. 56A-2-001. $[(CH_3)_3NH]_3Sb_2Cl_9$. Fragment of the structure, showing the atom numbering scheme, Sb coordination and hydrogen bonding [85Kal]. T = 296 K.

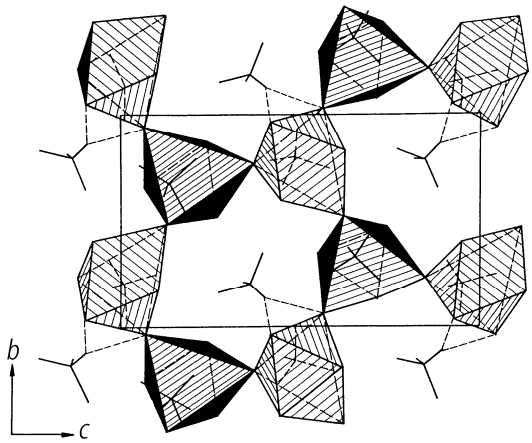

Fig. 56A-2-002. $[(CH_3)_3NH]_3Sb_2Cl_9$. Structure [85Kal]. T = 296 K. View along the *a* axis, showing two dimensional array of Sb_2Cl_9. $SbCl_6$ octahedra are represented by the surfaces and $(CH_3)_3NH$ tetrahedra by the bonds.

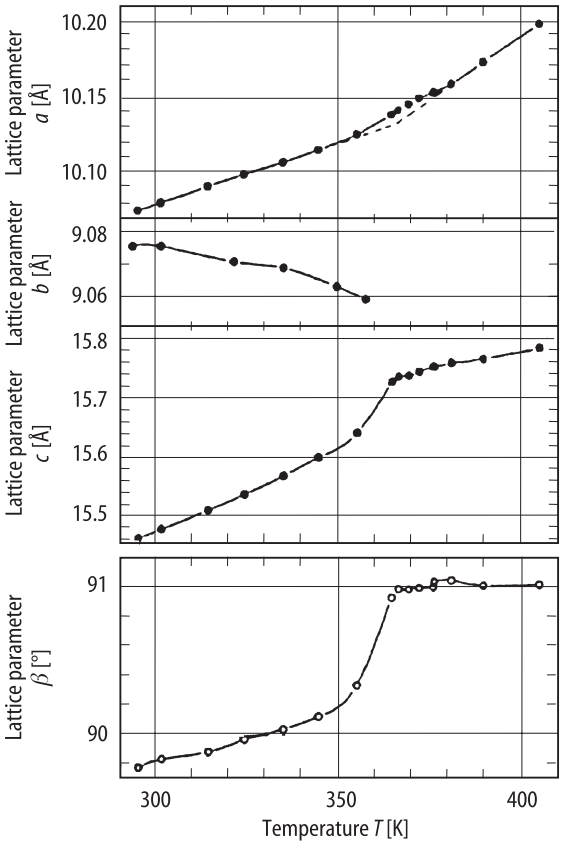

Fig. 56A-2-003. $[(CH_3)_3NH]_3Sb_2Cl_9$. *a*, *b*, *c*, β vs. *T* [95Tom]. *a*, *b*, *c*, β: lattice parameters.

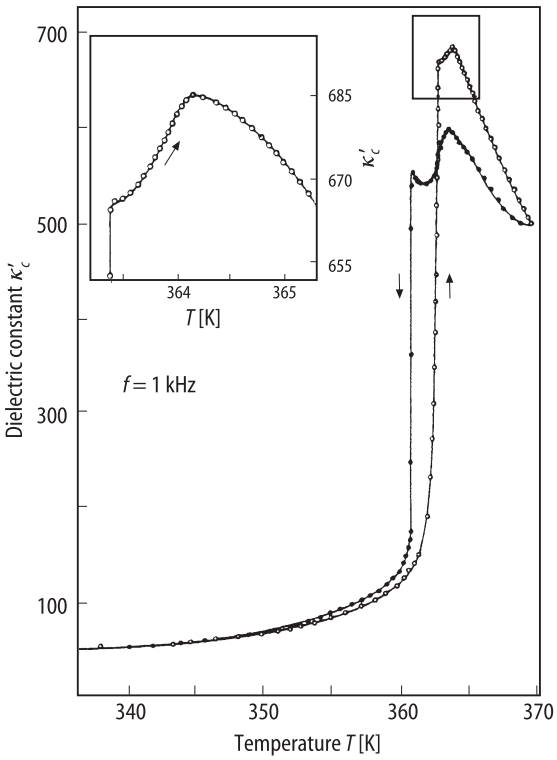

Fig. 56A-2-004. $[(CH_3)_3NH]_3Sb_2Cl_9$. κ_c' vs. T [89Jak].

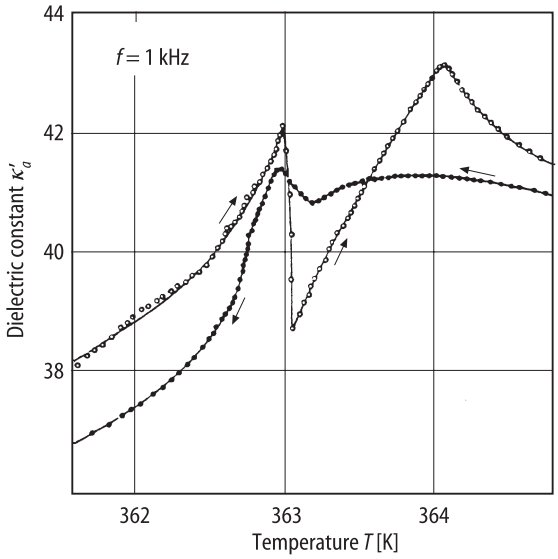

Fig. 56A-2-005. $[(CH_3)_3NH]_3Sb_2Cl_9$. κ_a' vs. T in the vicinity of Θ_t [89Jak].

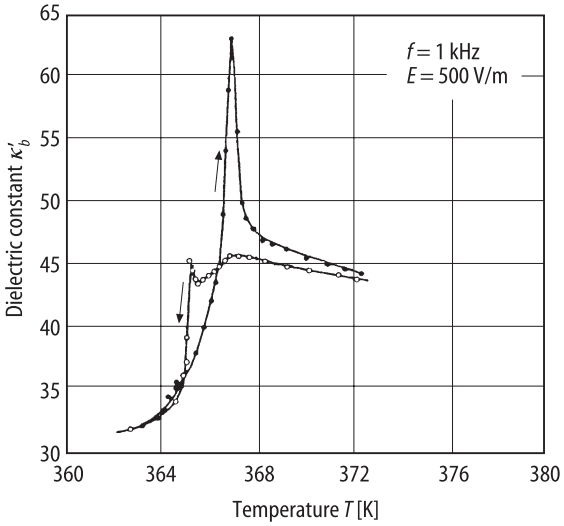

Fig. 56A-2-006. $[(CH_3)_3NH]_3Sb_2Cl_9$. κ'_b vs. T [86Jak1].

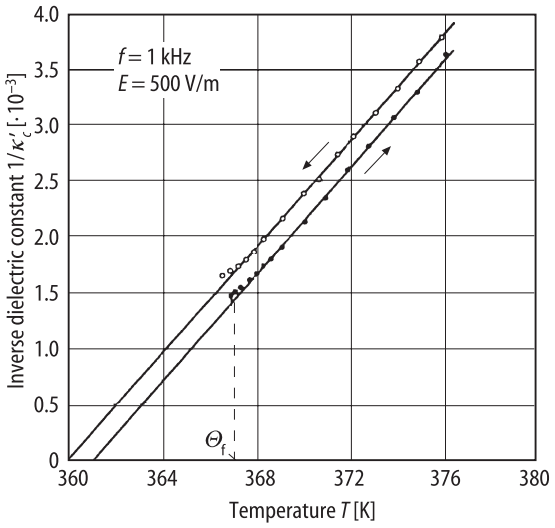

Fig. 56A-2-007. $[(CH_3)_3NH]_3Sb_2Cl_9$. $1/\kappa'_c$ vs. T [86Jak1].

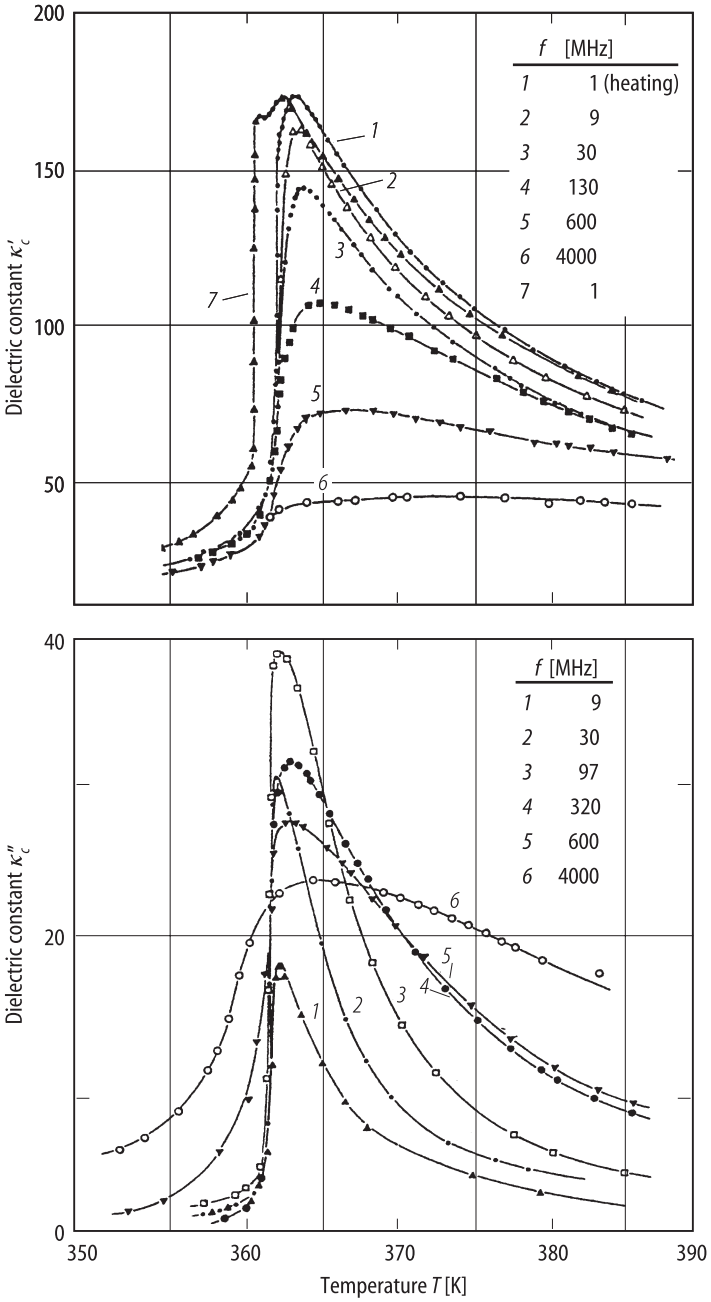

Fig. 56A-2-008. $[(CH_3)_3NH]_3Sb_2Cl_9$. κ_c', κ_c'' vs. T [92Sob]. Parameter: f.

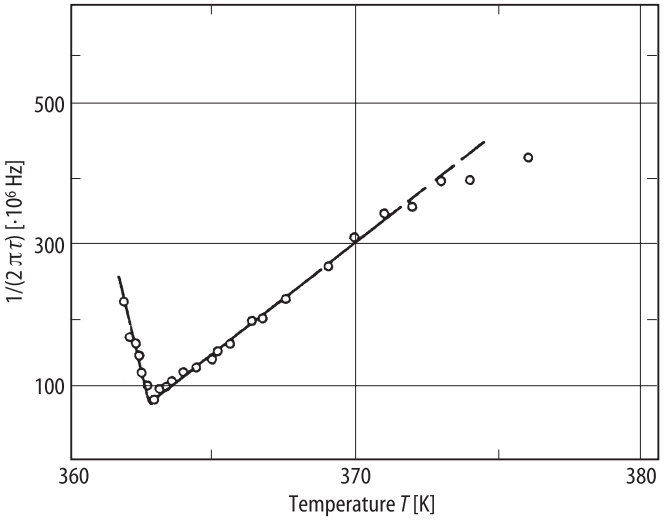

Fig. 56A-2-009. $[(CH_3)_3NH]_3Sb_2Cl_9$. $1/(2\pi\tau)$ vs. T [92Sob]. τ: relaxation time for low-frequency relaxation process.

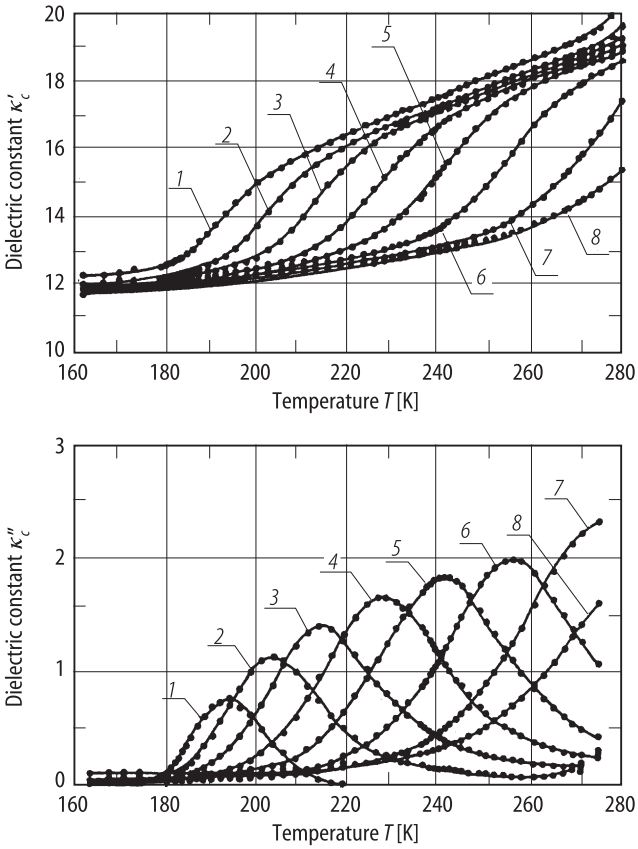

Fig. 56A-2-010. $[(CH_3)_3NH]_3Sb_2Cl_9$. κ_c', κ_c'' vs. T [93Bat]. Parameter: *f*. Curve *1*: f = 300 Hz, *2*: 1 kHz, *3*: 3 kHz, *4*: 10 kHz, *5*: 30 kHz, *6*: 100 kHz, *7*: 400 kHz, *8*: 1 MHz.

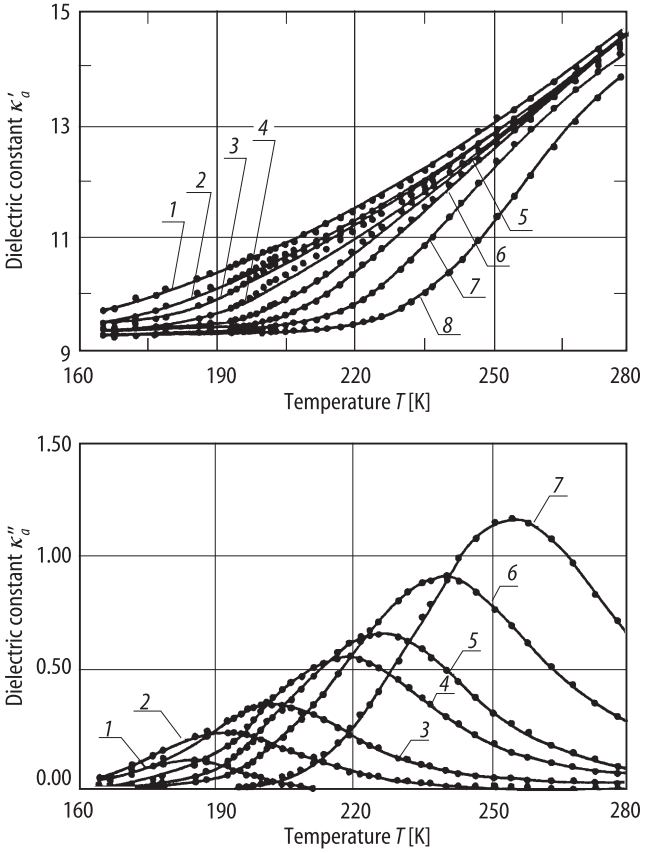

Fig. 56A-2-011. $[(CH_3)_3NH]_3Sb_2Cl_9$. κ'_a, κ''_a vs. T [93Bat]. Parameter: f. Curve *1*: f = 300 Hz, *2*: 1 kHz, *3*: 3 kHz, *4*: 10 kHz, *5*: 50 kHz, *6*: 100 kHz, *7*: 300 kHz, *8*: 1 MHz.

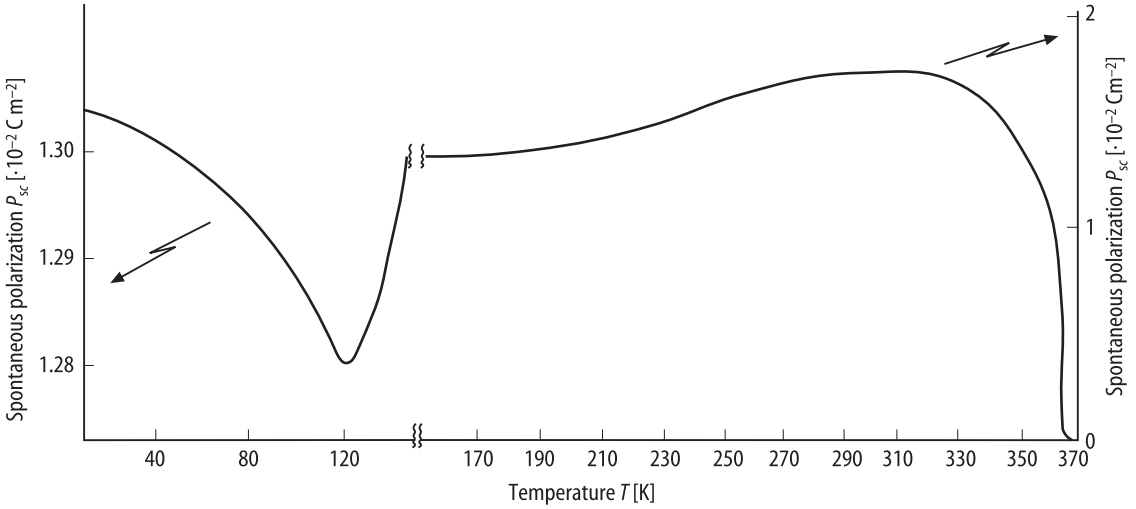

Fig. 56A-2-012. $[(CH_3)_3NH]_3Sb_2Cl_9$. P_{sc} vs. T [93Bat]. P_{sc}: spontaneous polarization along the c axis.

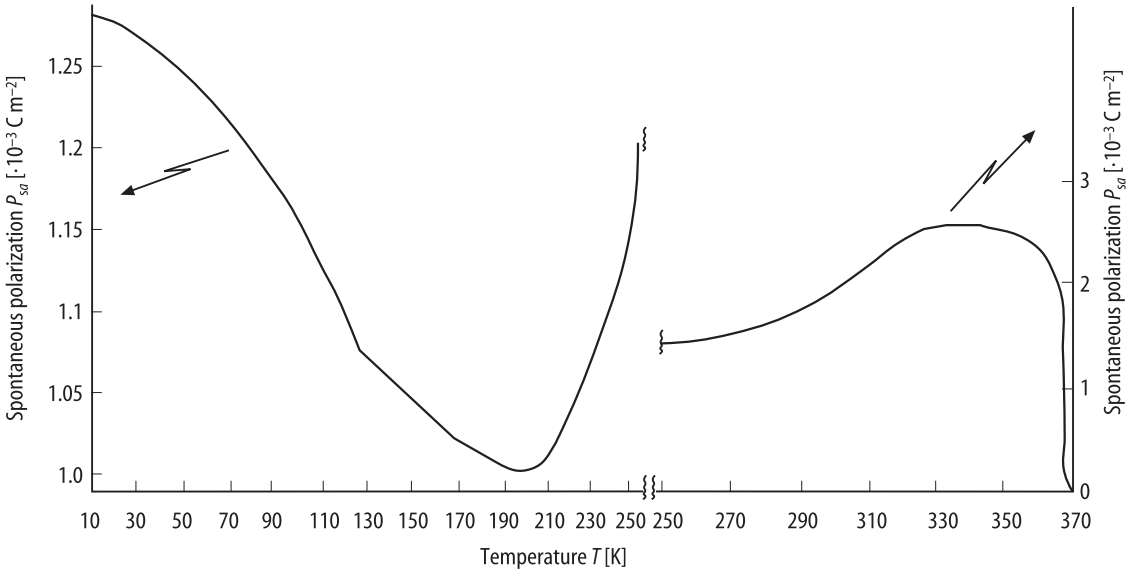

Fig. 56A-2-013. $[(CH_3)_3NH]_3Sb_2Cl_9$. P_{sa} vs. T [93Bat]. P_{sa}: spontaneous polarization along the a axis.

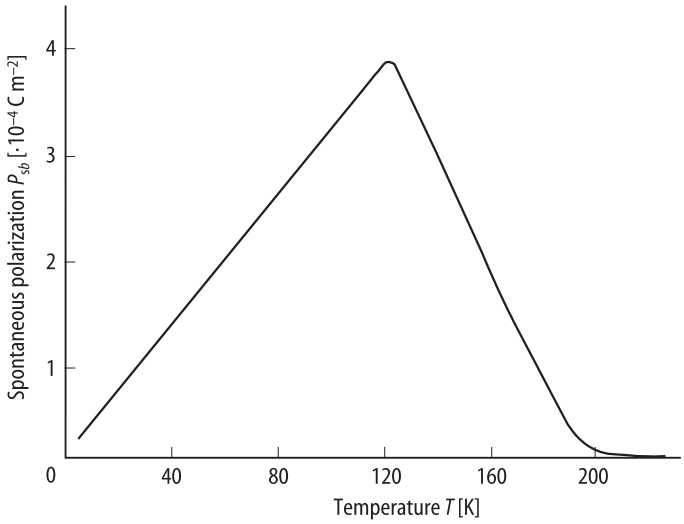

Fig. 56A-2-014. $[(CH_3)_3NH]_3Sb_2Cl_9$. P_{sb} vs. T [93Bat]. P_{sb}: spontaneous polarization along the b axis.

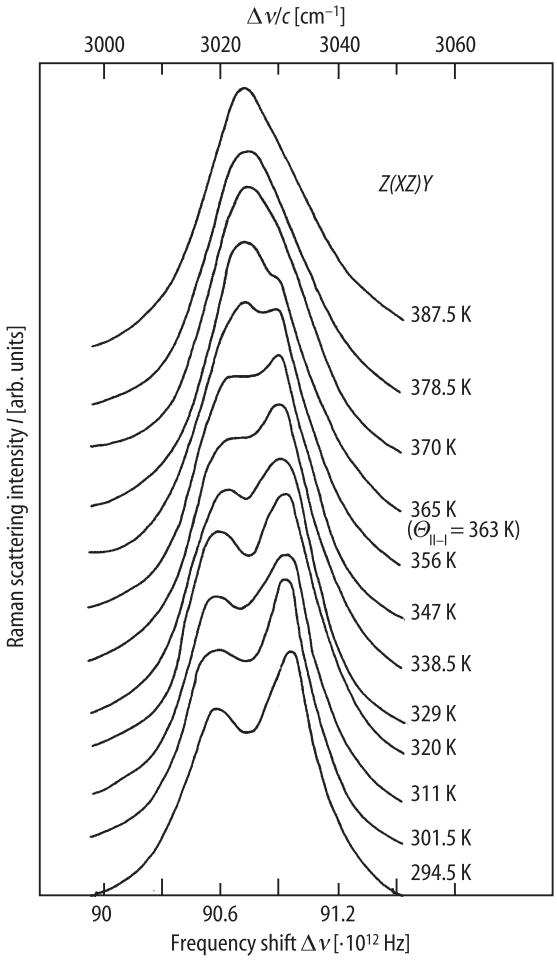

Fig. 56A-2-015. $[(CH_3)_3NH]_3Sb_2Cl_9$. *I* vs. $\Delta\nu$ [89Min2]. *I*: Raman scattering intensity observed in the *Z*(*XZ*)*Y* geometry. Parameter: *T*.

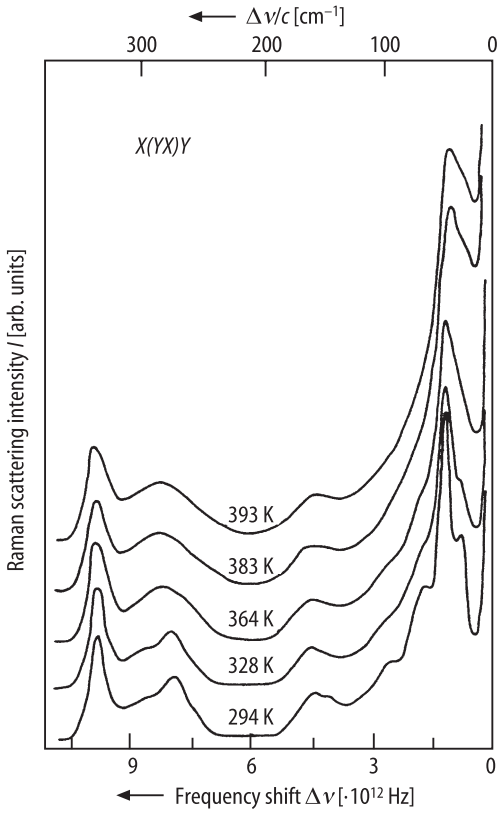

Fig. 56A-2-016. $[(CH_3)_3NH]_3Sb_2Cl_9$. I vs. $\Delta\nu$ [89Min2]. I: Raman scattering intensity observed in the $X(YX)Y$ geometry. Parameter: T.

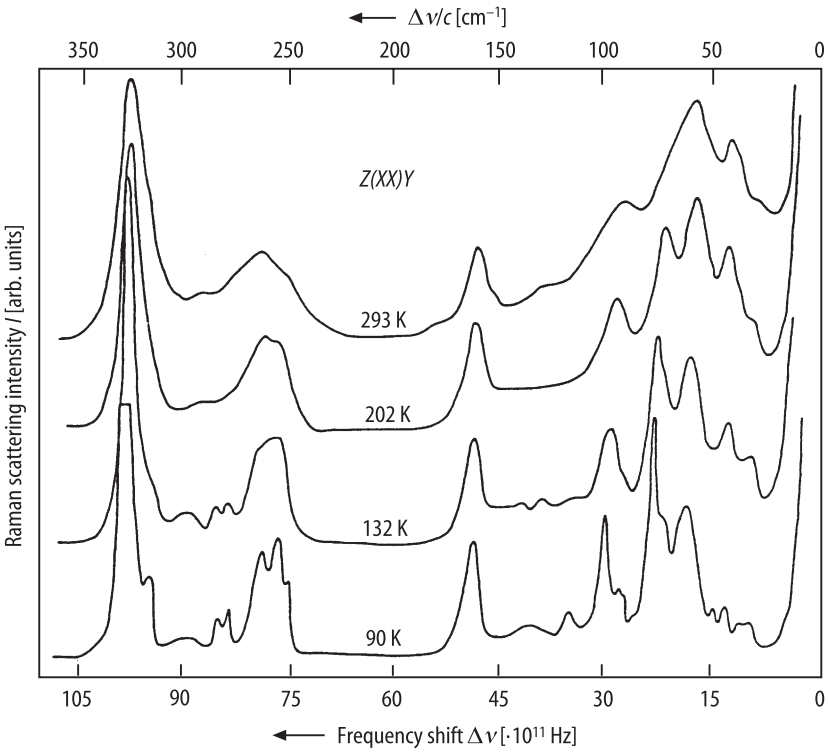

Fig. 56A-2-017. $[(CH_3)_3NH]_3Sb_2Cl_9$. I vs. $\Delta\nu$ [89Min2]. I: Raman scattering intensity observed in the $Z(XX)Y$ geometry. Parameter: T.

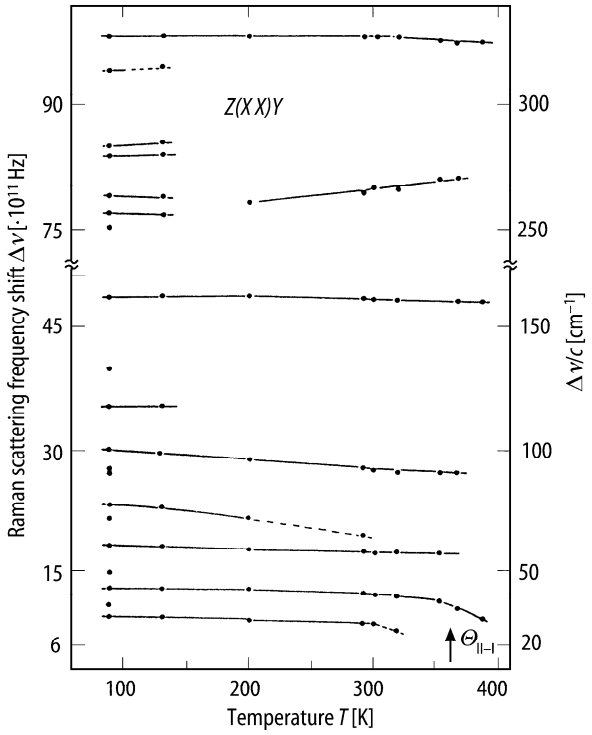

Fig. 56A-2-018. $[(CH_3)_3NH]_3Sb_2Cl_9$. $\Delta\nu$ vs. T [89Min2]. $\Delta\nu$: Raman scattering frequency shift observed in the $Z(XX)Y$ geometry.

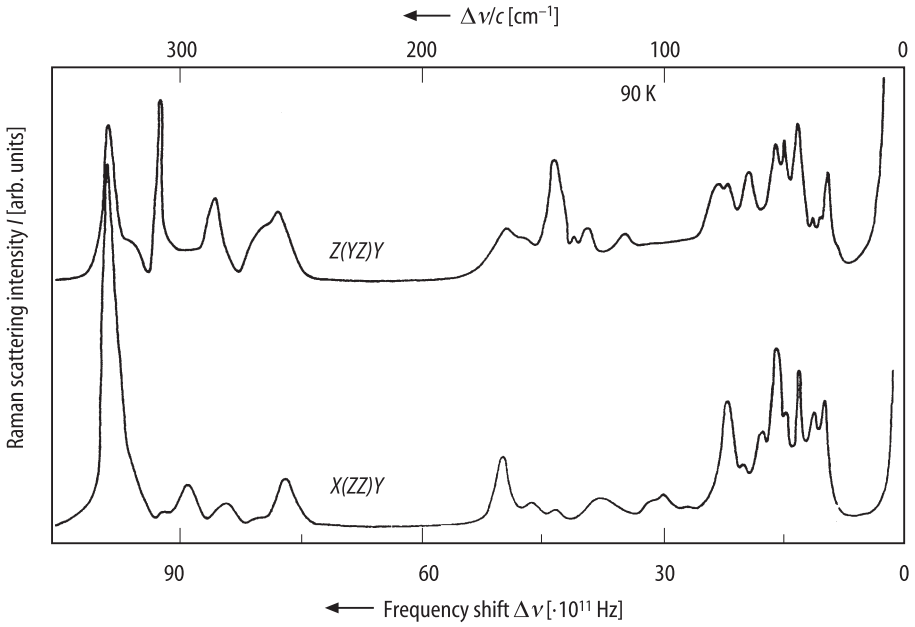

Fig. 56A-2-019. $[(CH_3)_3NH]_3Sb_2Cl_9$. I vs. $\Delta\nu$ [89Min2]. I: Raman scattering intensity observed at 90 K in the $Z(YZ)Y$ and $X(ZZ)Y$ geometries.

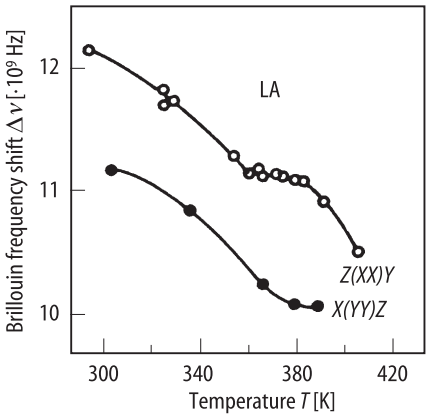

Fig. 56A-2-020. $[(CH_3)_3NH]_3Sb_2Cl_9$. $\Delta\nu$ vs. T [88Min]. $\Delta\nu$: Brillouin frequency shift of LA modes. Parameter: scattering geometry.

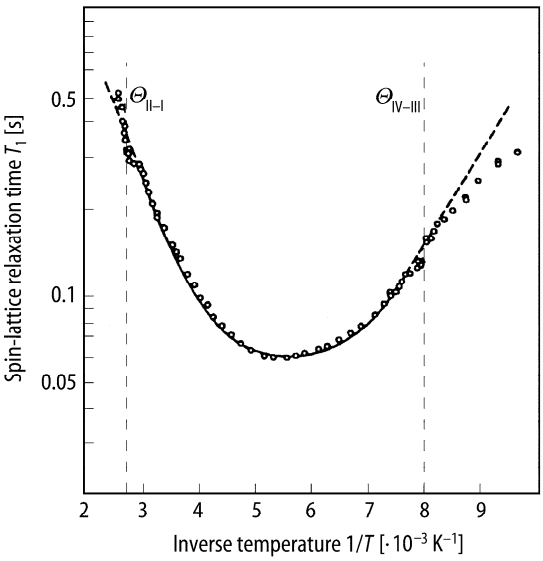

Fig. 56A-2-021. $[(CH_3)_3NH]_3Sb_2Cl_9$. T_1 vs. $1/T$ [87Idz]. T_1: proton spin-lattice relaxation time in powder. ν_L = 90 MHz.

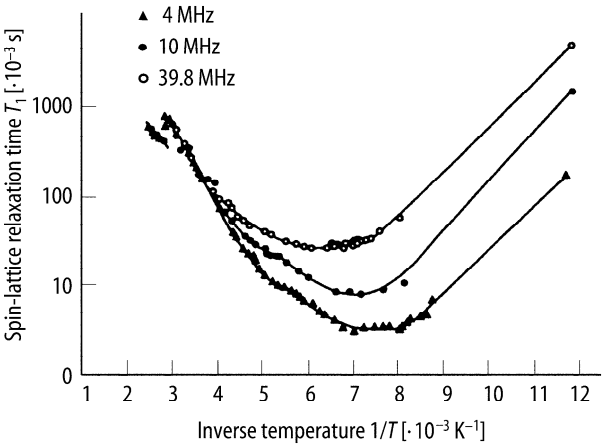

Fig. 56A-2-022. $[(CH_3)_3NH]_3Sb_2Cl_9$. T_1 vs. $1/T$ [93Jag]. T_1: proton spin-lattice relaxation time in powder. Full upside triangle: ν_L = 4 MHz, full circle: ν_L = 10 MHz, open circle: ν_L = 39.8 MHz.

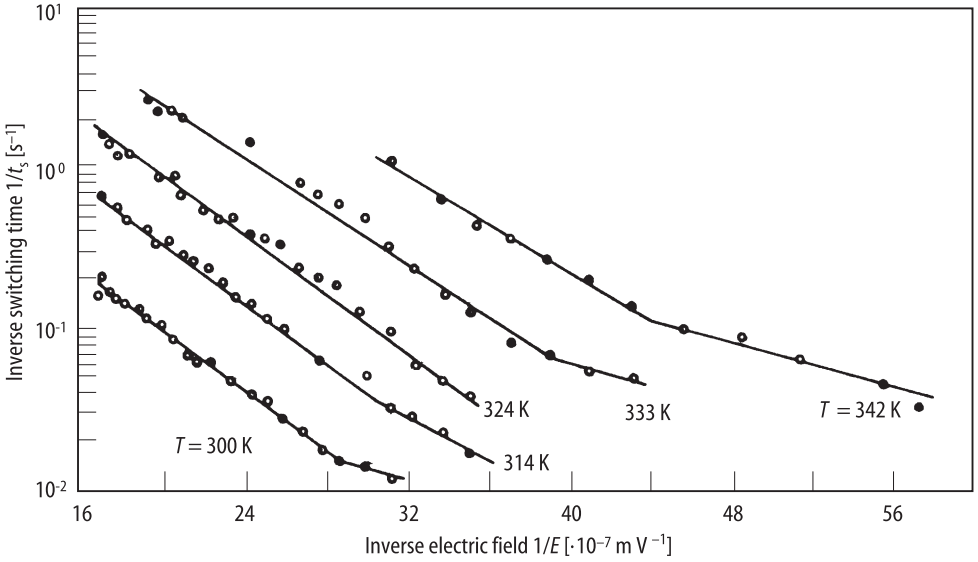

Fig. 56A-2-023. $[(CH_3)_3NH]_3Sb_2Cl_9$. $1/t_s$ vs. $1/E$ [92Pol]. t_s: switching time. Parameter: T.

References

85Kal Kallel, A., Bats, J.W.: Acta Crystallogr. Sect. C **41** (1985) 1022.
86Jak1 Jakubas, R., Czapla, Z., Galewski, Z., Sobczyk, L.: Ferroelectrics Lett. **5** (1986) 143.
86Jak2 Jakubas, R., Narewski, E., Sobczyk, L.: Phys. Status Solidi (a) **98** (1986) K115.
86Mro Mróz, J., Czapla, Z., Jakubas, R.: Acta Phys. Pol. A **70** (1986) 705.
87Idz Idziak, S., Jakubas, R.: Solid State Commun. **62** (1987) 171.
88Min Miniewicz, A., Jakubas, R., Ecolivet, C.: Ferroelectrics **80** (1988) 153.
89Jak Jakubas, R., Miniewicz, A., Bertault, M., Sworakowski, J.: J. Phys. (Paris) **50** (1989) 1483.
89Min1 Miniewicz, A., Sworakowski, J., Jakubas, R., Bertault, M., Ecolivet, C.: Ferroelectrics **94** (1989) 323.
89Min2 Miniewicz, A., Jakubas, R., Ecolivet, C., Girard, A.: J. Raman Spectrosc. **20** (1989) 381.
92Pol Połomska, M., Jakubas, R.: Ferroelectrics **126** (1992) 359.
92Prz Przesławski, J., Kosturek, B., Jakubas, R.: Ferroelectrics **126** (1992) 91.
92Sob Sobiestianskas, R., Czapla, Z., Jakubas, R.: Phys. Status Solidi (a) **130** (1992) K69.
92Urb Urban, S., Zając, W., Jakubas, R., Carlile, C.J., Gabryś, B.: Physica B **180** (1992) 1053.
92Var Varma, V., Bhattaacharjee, R., Vasan, H.N., Rao, C.N.R.: Spectrochim. Acta A **48** (1992) 1631.
93Bat Bator, G., Jakubas, R., Sobczyk, L., Mróz, J.: Ferroelectrics **141** (1993) 177.
93Jag Jagadeesh, B., Rajan, K., Venu, K., Sastry, V.S.S.: Solid State Commun. **86** (1993) 803.
95Tom Tomaszewski, P.E.: Acta Phys. Pol. **87** (1995) 631.

No. 56A-3 $[(CH_3)_2NH_2]_3Sb_2Br_9$, Dimethylammonium nonabromodiantimonate

(M = 1100.91)

1a	Ferroelectric activity in $[(CH_3)_2NH_2]_3Sb_2Br_9$ was discovered by Jakubas et al. in 1987.				87Jak
b	phase	III	II	I	87Jak
	state	F	P	P	
	crystal system			monoclinic	
	space group			$P2_1/a - C_{2h}^5$	
	Θ [K]		164	228	
	Spontaneous polarization was observed along the a, b and c axes. The highest value is along the c axis.				87Jak, 95Bat
	See Fig. 56A-3-011, Fig. 56A-3-012, Fig. 56A-3-013, Fig. 56A-3-014.				
	Yellow, transparent. Cleavage plane is nearly perpendicular to the c axis.				87Jak
	$\rho = 2.721 \cdot 10^3$ kg m^{-3}.				87Jak
	Some decomposition at 130...135 °C and the residue melts at 258...260 °C.				87Jak
2a	Material preparation: precipitated from an aqueous solution of stoichiometric amounts of Sb_2O_3 and $NH_2(CH_3)_2Br$ with great excess of HBr.				
	Crystal growth: in a saturated acetonitrile solution at room temperature.				94Bat2
	See also				87Jak
3a	Unit cell parameters in phase I: a = 14.612(8) Å, b = 9.228(4) Å, c = 10.005(8) Å, β = 94.91(6)° at RT.				87Jak
b	Z = 2 in phase I.				87Jak
4	Thermal expansion: Fig. 56A-3-001.				
5a	Dielectric constant: Fig. 56A-3-002, Fig. 56A-3-003, Fig. 56A-3-004, Fig. 56A-3-005, Fig. 56A-3-006.				
	Dielectric dispersion: Fig. 56A-3-007, Fig. 56A-3-008, Fig. 56A-3-009, Fig. 56A-3-010.				
c, d	Spontaneous polarization and pyroelectric coefficient: Fig. 56A-3-011, Fig. 56A-3-012, Fig. 56A-3-013, Fig. 56A-3-014.				
6a	Heat capacity: see				92Min
9a	Infrared absorption: see				92Mar, 94Bat1, 94Bat2
10b	Brillouin scattering: Fig. 56A-3-015, Fig. 56A-3-016.				
13a	NMR: Fig. 56A-3-017.				

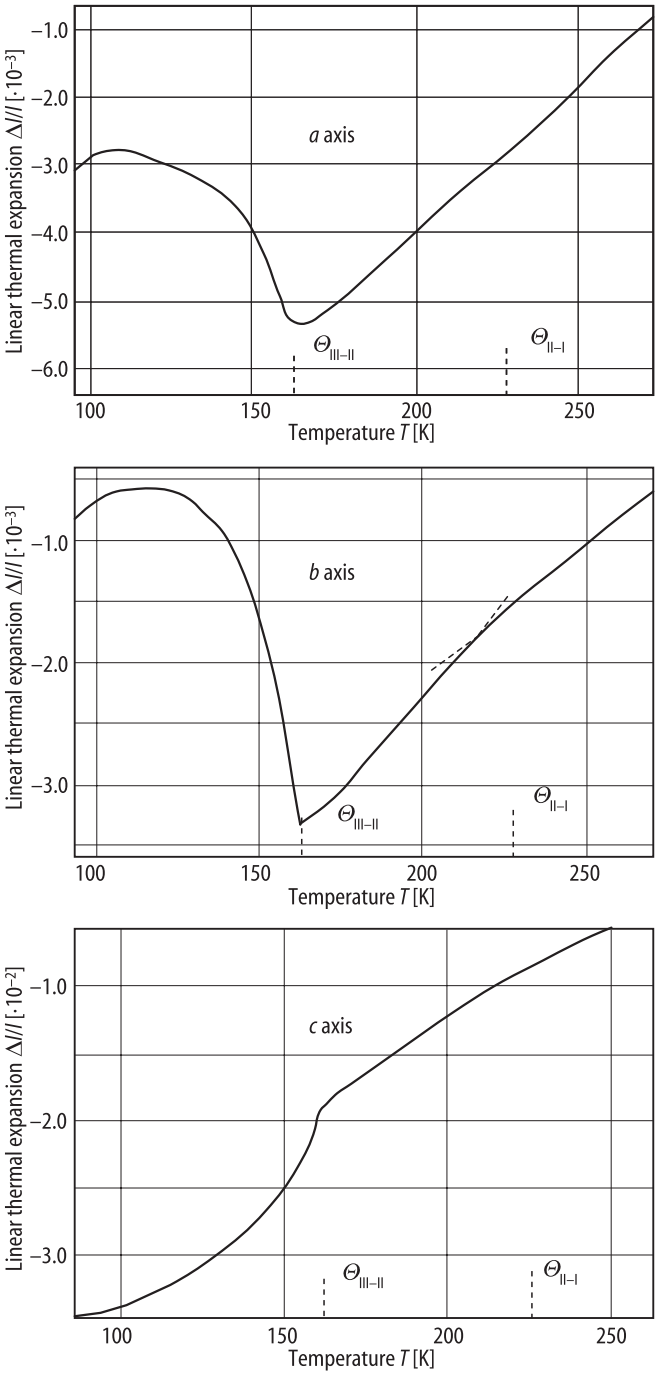

Fig. 56A-3-001. $[(CH_3)_2NH_2]_3Sb_2Br_9$. $\Delta l/l$ vs. T [95Jak]. $\Delta l/l$: linear thermal expansion along the a, b and c axes.

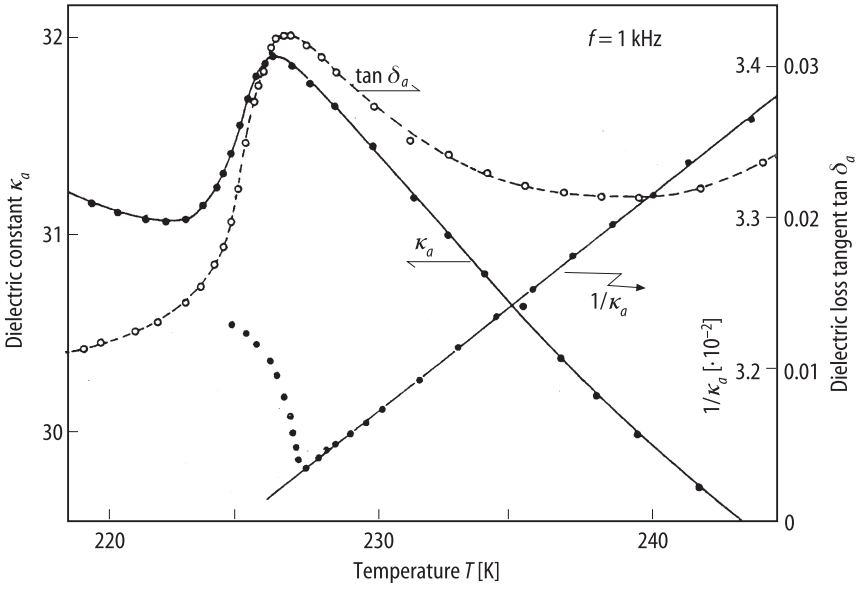

Fig. 56A-3-002. $[(CH_3)_2NH_2]_3Sb_2Br_9$. κ_a, $1/\kappa_a$, tan δ_a vs. T in the vicinity of Θ_{II-I} [87Jak].

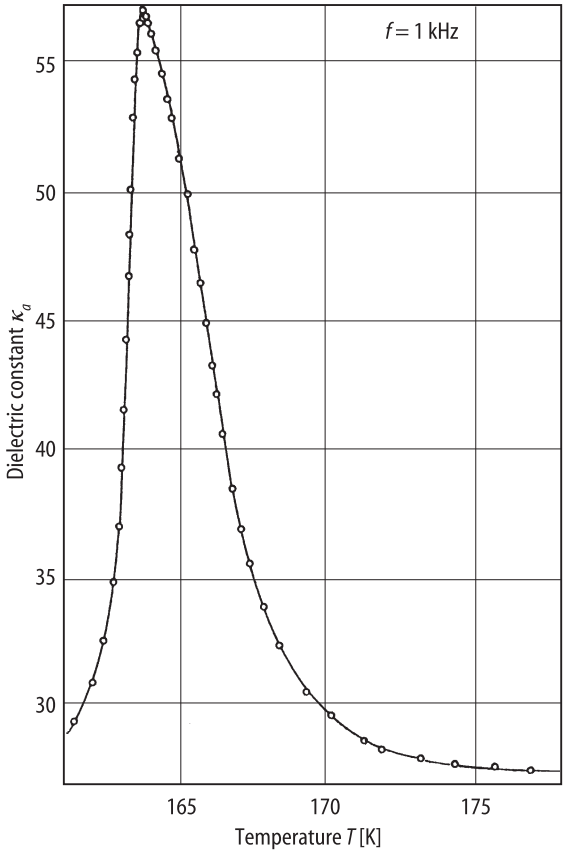

Fig. 56A-3-003. $[(CH_3)_2NH_2]_3Sb_2Br_9$. κ_a vs. T in the vicinity of Θ_{III-II} [87Jak].

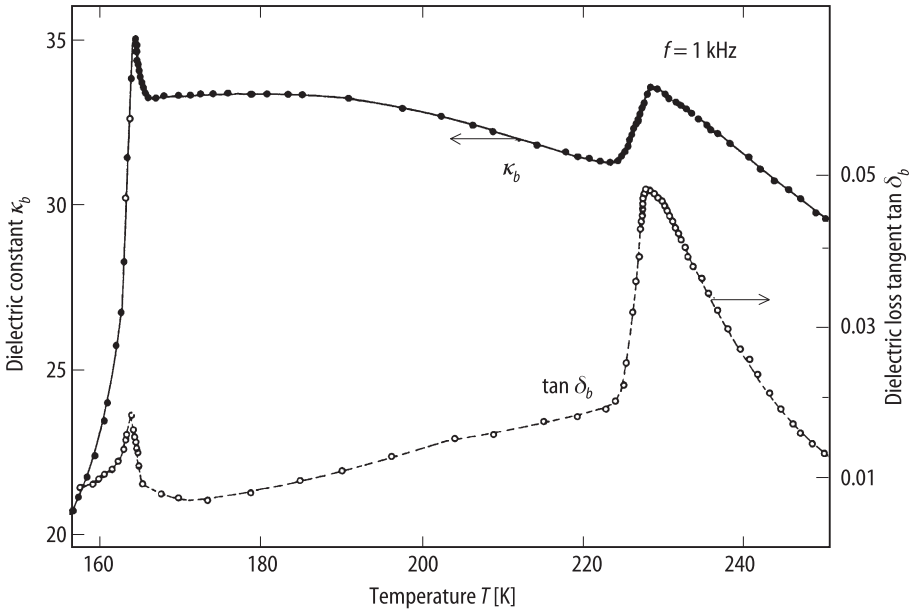

Fig. 56A-3-004. $[(CH_3)_2NH_2]_3Sb_2Br_9$. κ_b, tan δ_b vs. T [87Jak].

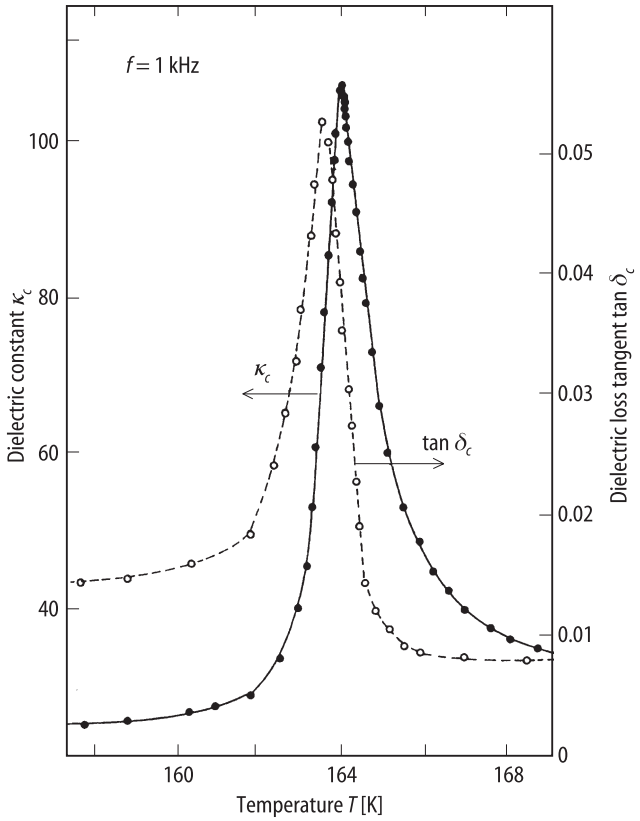

Fig. 56A-3-005. $[(CH_3)_2NH_2]_3Sb_2Br_9$. κ_c, tan δ_c vs. T in the vicinity of Θ_{II-II} [87Jak].

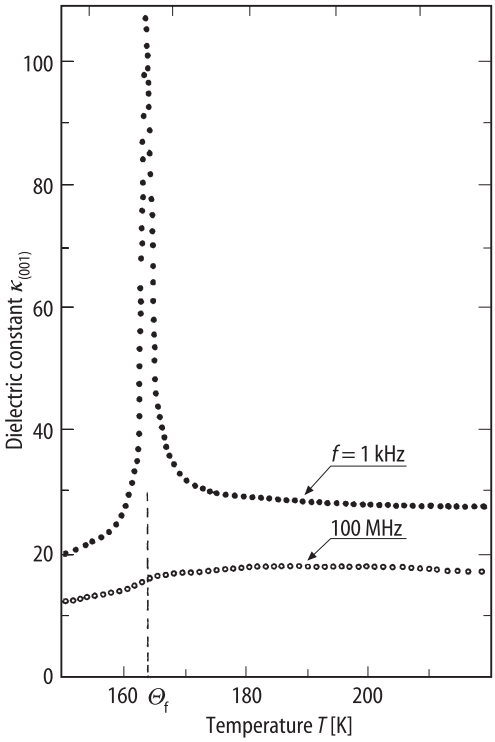

Fig. 56A-3-006. $[(CH_3)_2NH_2]_3Sb_2Br_9$. $\kappa_{(001)}$ vs. T [87Jak]. Parameter: f. $\kappa_{(001)}$: dielectric constant of (001) plate specimen.

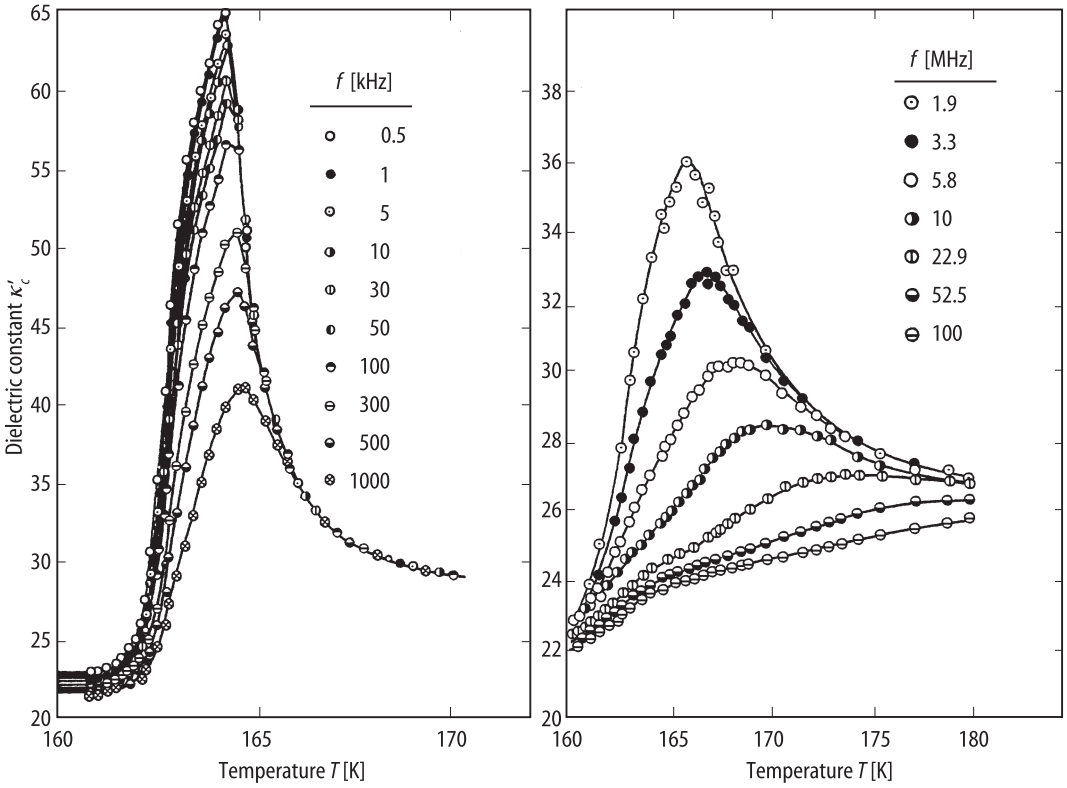

Fig. 56A-3-007. $[(CH_3)_2NH_2]_3Sb_2Br_9$. κ'_c vs. T [95Bat]. Parameter: f.

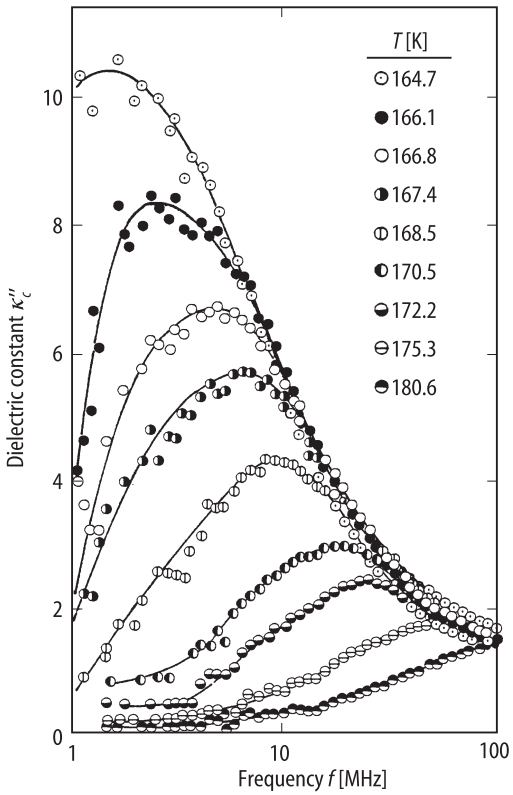

Fig. 56A-3-008. $[(CH_3)_2NH_2]_3Sb_2Br_9$. κ_c'' vs. f [95Bat]. Parameter: T.

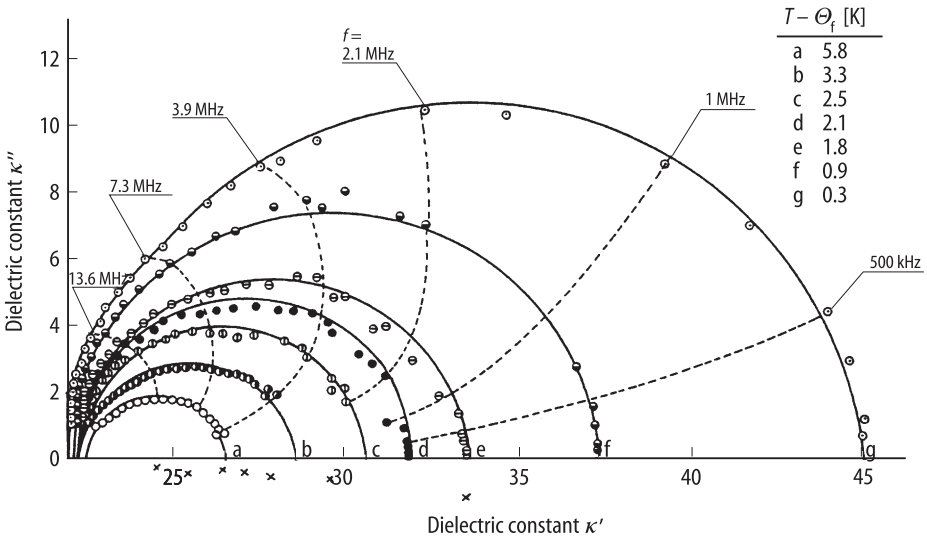

Fig. 56A-3-009. $[(CH_3)_2NH_2]_3Sb_2Br_9$. Cole-Cole plot of complex dielectric constant [95Bat]. Parameter: $T - \Theta_f$. ×: center of Cole-Cole arc.

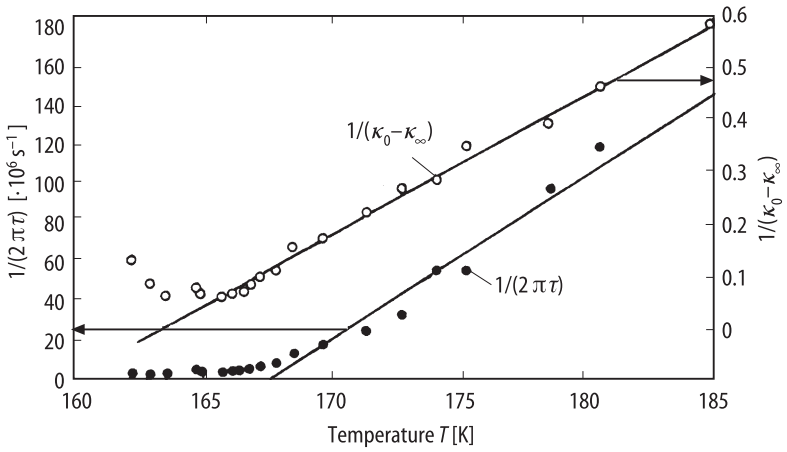

Fig. 56A-3-010. $[(CH_3)_2NH_2]_3Sb_2Br_9$. $1/(2\pi\tau)$, $1/(\kappa_0 - \kappa_\infty)$ vs. T [95Bat]. τ: dielectric relaxation time, κ_0, κ_∞: static and high frequency dielectric constant.

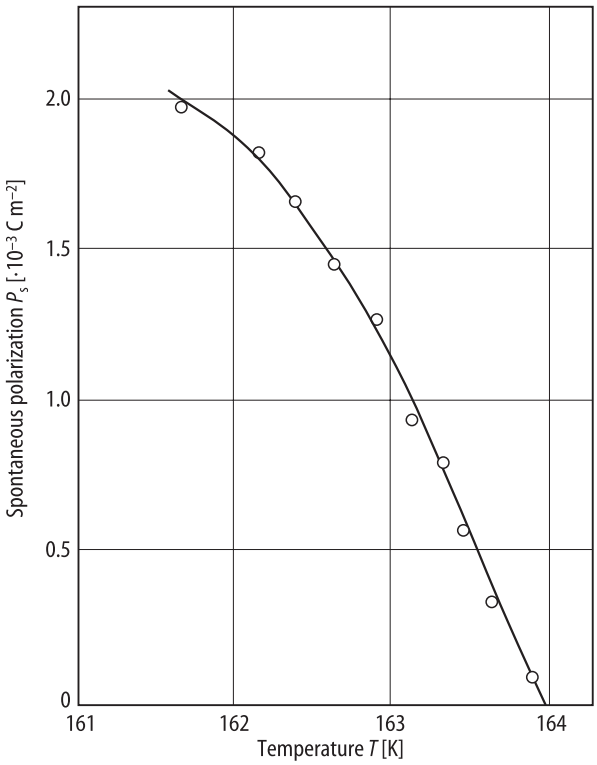

Fig. 56A-3-011. $[(CH_3)_2NH_2]_3Sb_2Br_9$. P_s vs. T [87Jak]. P_s: spontaneous polarization along the c axis.

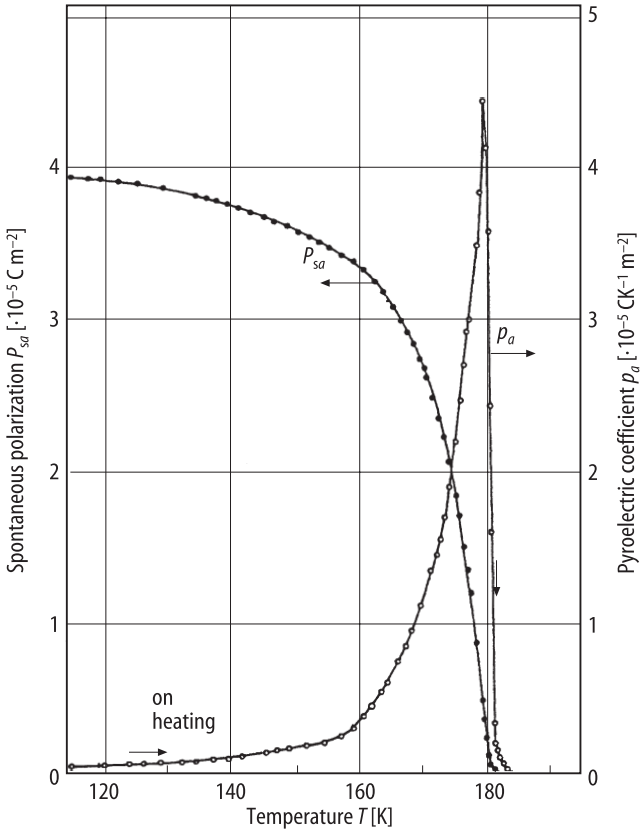

Fig. 56A-3-012. $[(CH_3)_2NH_2]_3Sb_2Br_9$. p_a, P_{sa} vs. T [88Min]. p_a, P_{sa}: pyroelectric coefficient, spontaneous polarization along the a axis. Note a large overheating of phase III.

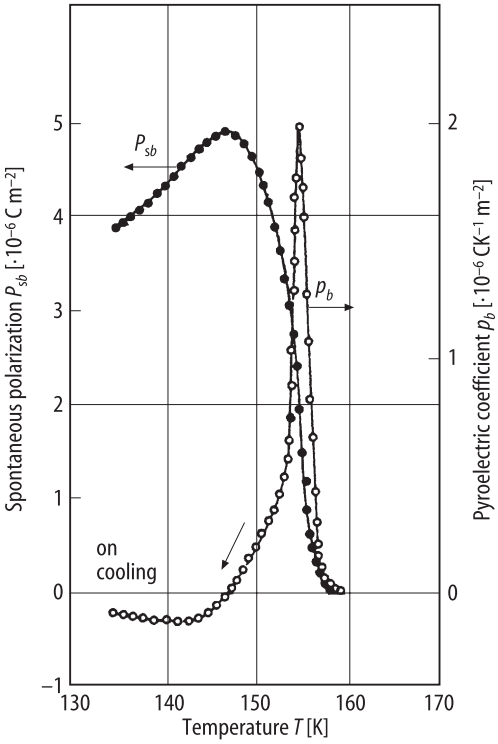

Fig. 56A-3-013. $[(CH_3)_2NH_2]_3Sb_2Br_9$. p_b, P_{sb} vs. T [88Min]. p_b, P_{sb}: pyroelectric coefficient, spontaneous polarization along the *b* axis.

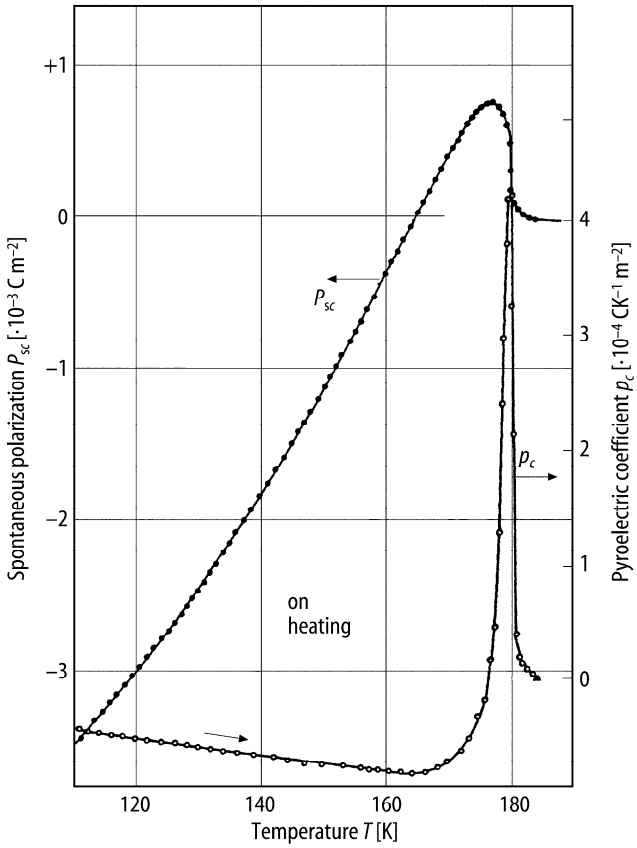

Fig. 56A-3-014. $[(CH_3)_2NH_2]_3Sb_2Br_9$. p_c, P_{sc} vs. T [88Min]. p_c, P_{sc}: pyroelectric coefficient, spontaneous polarization along the c axis. Note a large overheating of phase III.

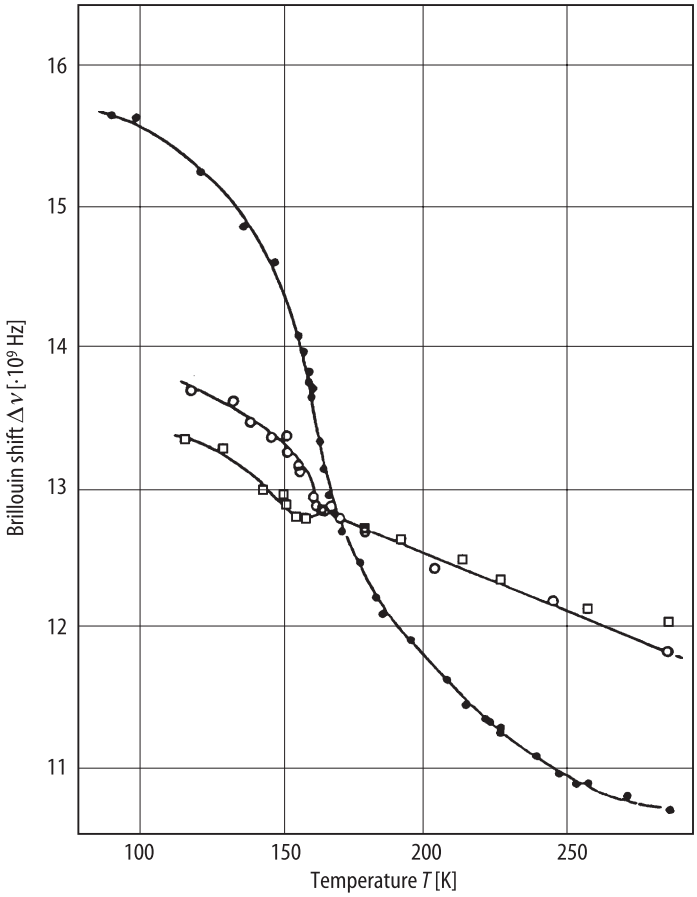

Fig. 56A-3-015. $[(CH_3)_2NH_2]_3Sb_2Br_9$. $\Delta\nu$ vs. T [89Eco]. $\Delta\nu$: Brillouin shift of the LA mode. Parameter: propagation direction, $\boldsymbol{q} \parallel \boldsymbol{c}$ (full circle), $\boldsymbol{q} \parallel \mathbf{a}$ (open square), $\boldsymbol{q} \parallel \boldsymbol{b}$ (open circle).

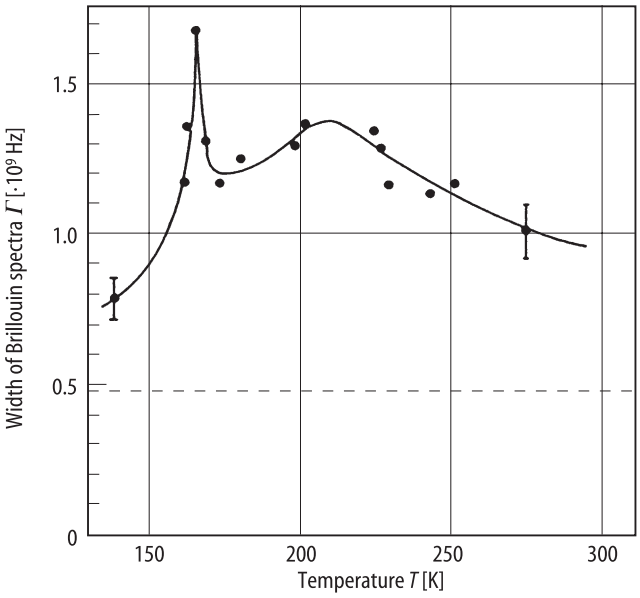

Fig. 56A-3-016. $[(CH_3)_2NH_2]_3Sb_2Br_9$. Γ vs. T [89Eco]. Γ: width of Brillouin spectra of the LA mode. Dashed line indicates the instrumental width.

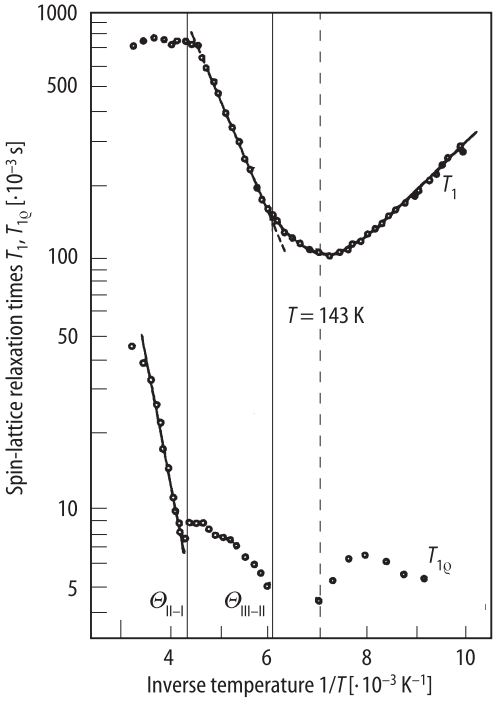

Fig. 56A-3-017. $[(CH_3)_2NH_2]_3Sb_2Br_9$. T_1, $T_{1\rho}$ vs. $1/T$ [88Idz]. T_1 and $T_{1\rho}$ are spin-lattice relaxation times of proton in laboratory frame and rotating frame, respectively. ν_L = 90 MHz.

References

87Jak Jakubas, R., Sobczyk, L., Matuszewski, J.: Ferroelectrics **74** (1987) 339.
88Idz Idziak, S., Jakubas, R.: Ferroelectrics **80** (1988) 75.
88Min Miniewicz, A., Jakubas, R.: Solid State Commun. **67** (1988) 1079.
89Eco Ecolivet, C., Miniewicz, A., Jakubas, R.: Solid State Commun. **71** (1989) 143.
92Mar Marqueton, Y., Miniewicz, A., Jakubas, R.: J. Raman Spectrosc. **23** (1992) 347.
92Min Miniewicz, A., Sworakowski, J., Bertault, M., Jakubas, R.: Ferroelectrics **125** (1992) 39.
94Bat1 Bator, G., Jakubas, R., Baran, J., Sobczyk, L.: Ferroelectrics **152** (1994) 267.
94Bat2 Bator, G., Baran, J., Jakubas, R., Ratajczak, H.: Vibrational Spectrosc. **6** (1994) 193.
95Bat Bator, G., Jakubas, R.: Phys. Status Solidi (a) **147** (1995) 591.
95Jak Jakubas, R., Mróz, J., François, P., Lefebvre, J.: Ferroelectrics **173** (1995) 221.

No. 56A-4 $(CH_3NH_3)_3Sb_2Br_9$, Methylammonium nonabromodiantimonate

(M = 1058.83)

1a Polarization reversal in $(CH_3NH_3)_3Sb_2Br_9$ by poling was first reported by Mróz et al. in 1994. Pyroelectric activity was also reported below an upper transition temperature at 168 K by Jakubas in 1986. 94Mro 86Jak

b

phase	III	II	I	86Jak
state	F [a])		P	[a]) 94Mro
crystal system			trigonal	[b]) 85Jak
space group			$P\bar{3}m1 - D_{3d}^3$ [b]) [c])	[c]) 92Ish
Θ [K]	131	168		85Jak
	$[(CH_3ND_3)_3Sb_2Br_9$: 129	166] [d])		[d]) 90Mac

P_s || [100] in phase III. 94Mro
Bright yellow in color. 92Ish
Cleavage plane ⊥ to the c axis for hexagonal cell. 94Mro
Phase diagram in regard to p: Fig. 56A-4-001.
$\rho = 2.95 \cdot 10^3$ kg m^{-3}, $\rho_X = 3.049(2) \cdot 10^3$ kg m^{-3}. 92Ish

2a Crystal growth: slow evaporation of an aqueous solution containing stoichiometric molar ratio of $CH_3NH_2 \cdot HBr$ and $SbBr_3$ with a large excess of HBr. 86Jak

b Crystal form: Fig. 56A-4-002.

3a Unit cell parameters: a = 8.188(2) Å, c = 9.927(3) Å at 300K for hexagonal cell. 92Ish

b Z = 1 in phase I. 85Jak
Crystal structure: Table 56A-4-001, Table 56A-4-002.

4 Thermal expansion: Fig. 56A-4-003.

5a Dielectric constant: Fig. 56A-4-004.
Dielectric dispersion: Fig. 56A-4-005, Fig. 56A-4-006, Fig. 56A-4-007.

c Spontaneous polarization: Fig. 56A-4-008, Fig. 56A-4-009.

d Pyroelectric coefficient: Fig. 56A-4-008.

6a Heat capacity: see 92Jak

9a Infrared transmission: see 93Jak

13a NMR: Fig. 56A-4-010, Fig. 56A-4-011.
NQR: Fig. 56A-4-012, Fig. 56A-4-013, Fig. 56A-4-014, Fig. 56A-4-015.

Table 56A-4-001. $(CH_3NH_3)_3Sb_2Br_9$. Crystal structure of phase I [92Ish]. Fractional coordinates and anisotropic temperature parameters. U_{ij} is defined by Eq. (d) in Introduction. The values of U_{ij} are given in 10^{-4} Å^2. T = 300 K. An approximate position of the cation $CH_3NH_3^+$ is at (0, 0, 0) from the difference Fourier maps.

Atom	Position [a])	x	y	z	U_{11}	U_{22}	U_{33}	U_{12}	U_{13}	U_{23}
Sb	2d	0.6667	0.3333	–0.1861(3)	380(11)	380(11)	304(14)	190(6)	0	0
Br(1)	3e	0.5000	0.5000	0.0000	981(33)	533(28)	819(33)	267(14)	138(12)	275(25)
Br(2)	6i	0.3573(5)	0.1787(2)	–0.3319(3)	650(18)	650(18)	697(23)	21(30)	–302(17)	302(17)

[a]) Wyckoff notation: 6i: $x, \bar{x}, z$; $x, 2x, z$; $2\bar{x}, \bar{x}, z$; $\bar{x}, x, \bar{z}$; $\bar{x}, 2\bar{x}, \bar{z}$; $2x, x, \bar{z}$.
3e: 1/2, 0, 0; 0, 1/2, 0; 1/2, 1/2, 0.
2d: 1/3, 2/3, z; 2/3, 1/3, $\bar{z}$.

Table 56A-4-002. $(CH_3NH_3)_3Sb_2Br_9$. Crystal structure of phase I [92Ish]. Bond distances [Å] and angles [°]. T = 300 K.

Sb–Br(1) [a])	3.000(3)
Sb–Br(2) [b])	2.628(5)
Sb–Br(1)–Sb(^{i}) [c])	180.0
Br(2)–Sb–Br(2^{ii})	92.6(2)
Br(1)–Sb–Br(2)	90.6(1)
Br(1)–Sb–Br(1^{iii})	86.1(1)
Br(1)–Sb–Br(2^{ii})	175.1(2)

[a]) The bridging bromine atom.
[b]) The terminal bromine atom.
[c]) Atoms carrying i, ii, and iii are related to original atoms by the relationships
2/3, 1/3, $\bar{z} \rightarrow$ 1/3, 2/3, z; $2x, x, \bar{z} \rightarrow \bar{x}, x, \bar{z}$;
1/2, 1/2, 0 → 1/2, 0, 0, respectively.

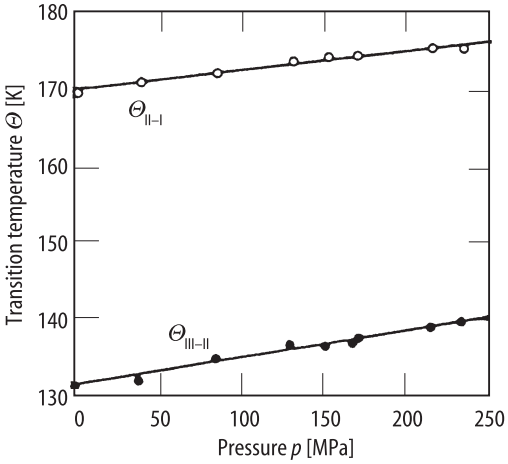

Fig. 56A-4-001. $(CH_3NH_3)_3Sb_2Br_9$. Θ_{II-I}, Θ_{III-II} vs. p [90Koz].

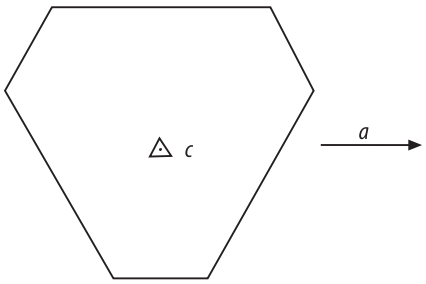

Fig. 56A-4-002. $(CH_3NH_3)_3Sb_2Br_9$. Crystal form [85Jak]. Hexagonal plate.

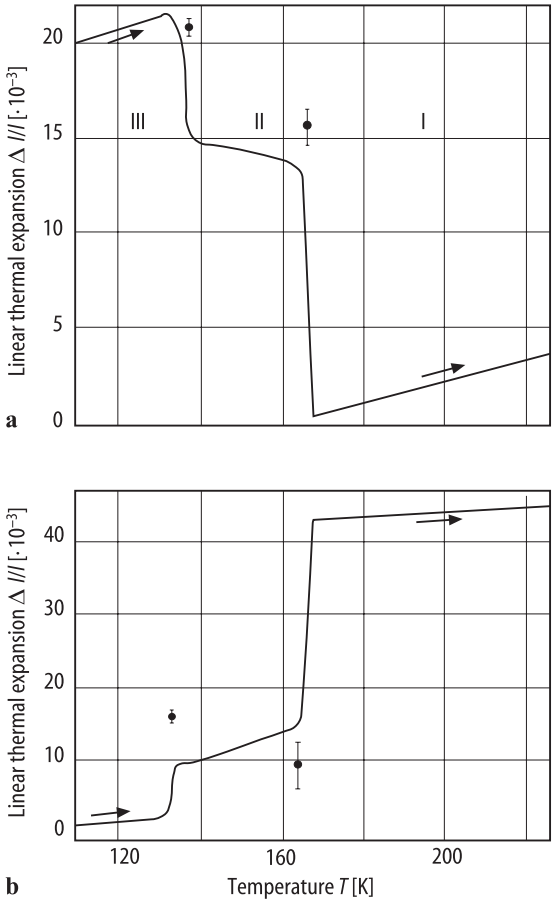

Fig. 56A-4-003. $(CH_3NH_3)_3Sb_2Br_9$. $\Delta l/l$ vs. T [92Jak]. $\Delta l/l$: linear thermal expansion (**a**) along the a axis, (**b**) along the c axis.

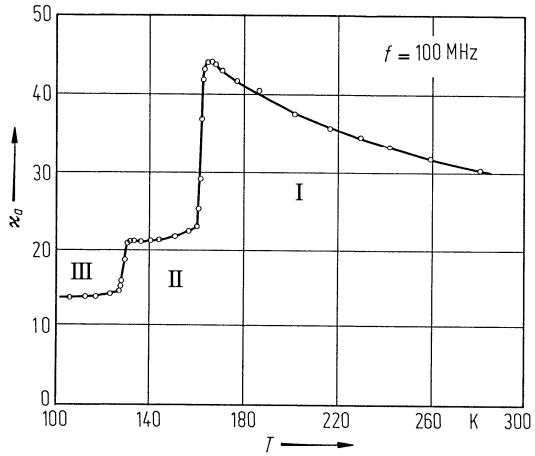

Fig. 56A-4-004. $(CH_3NH_3)_3Sb_2Br_9$. κ_a vs. T [86Jak].

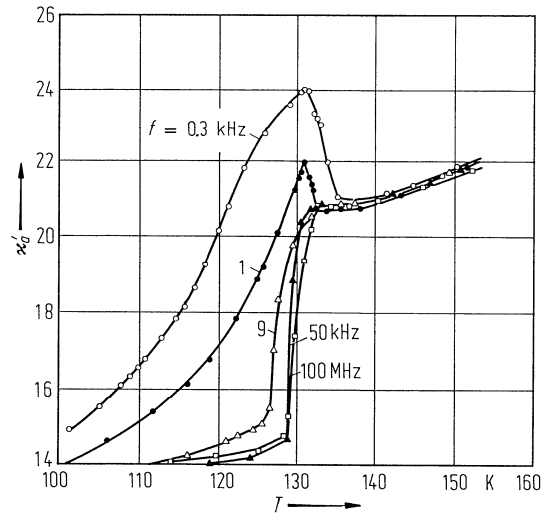

Fig. 56A-4-005. $(CH_3NH_3)_3Sb_2Br_9$. κ'_a vs. T near Θ_{III-II} [86Jak]. Parameter: f.

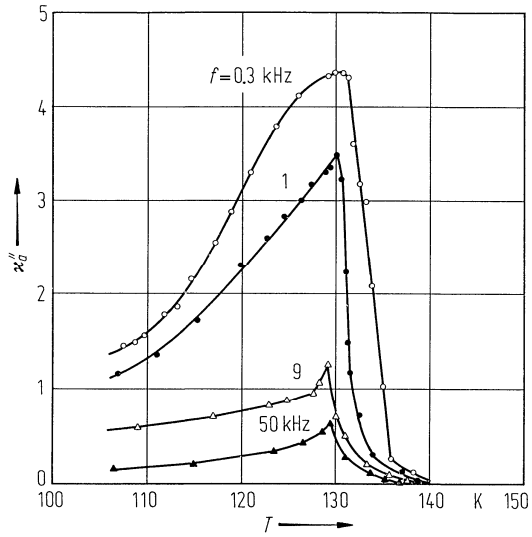

Fig. 56A-4-006. $(CH_3NH_3)_3Sb_2Br_9$. κ''_a vs. T near Θ_{III-II} [86Jak]. Parameter: f.

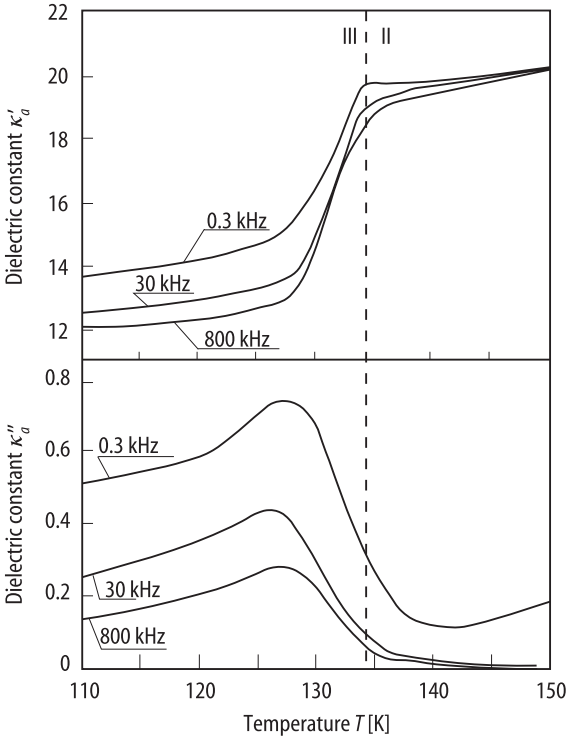

Fig. 56A-4-007. $(CH_3NH_3)_3Sb_2Br_9$. κ'_a, κ''_a vs. T near Θ_{III-II} [94Jak]. Parameter: f.

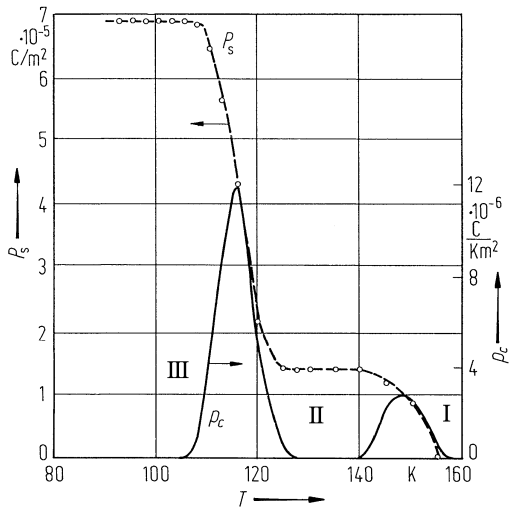

Fig. 56A-4-008. $(CH_3NH_3)_3Sb_2Br_9$. p_c, P_s vs. T [86Jak]. p_c: pyroelectric coefficient along the c axis.

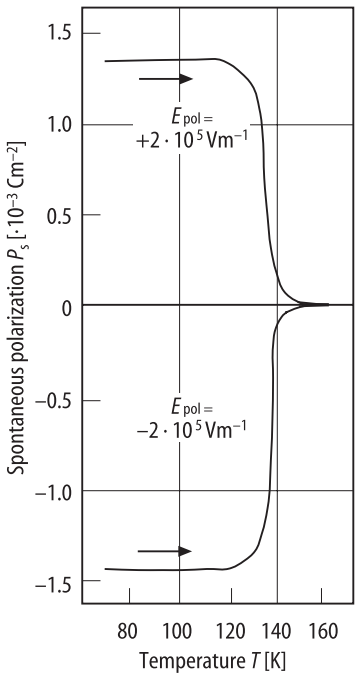

Fig. 56A-4-009. $(CH_3NH_3)_3Sb_2Br_9$. P_s vs. T [94Mro]. Parameter: E_{pol}. E_{pol}: poling field.

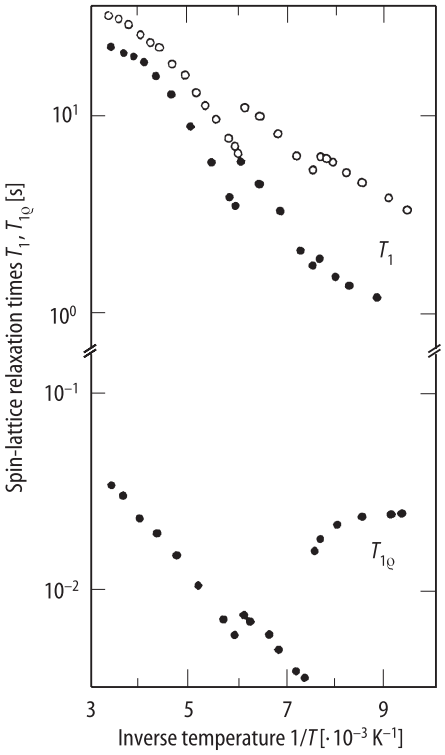

Fig. 56A-4-010. $(CH_3NH_3)_3Sb_2Br_9$, $(CH_3ND_3)_3Sb_2Br_9$. T_1, $T_{1\rho}$ vs. $1/T$ [90Mac]. T_1 and $T_{1\rho}$ are spin-lattice relaxation times of proton in laboratory frame and rotating frame, respectively. ν_L = 200 MHz. Full circle: $(CH_3NH_3)_3Sb_2Br_9$, open circle: $(CH_3ND_3)_3Sb_2Br_9$. Polycrystalline specimens. The estimated rate of deuteration was more than 99%.

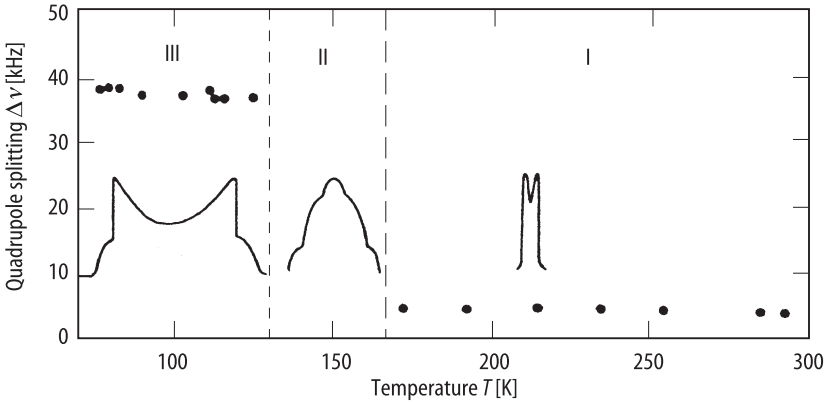

Fig. 56A-4-011. $(CH_3ND_3)_3Sb_2Br_9$. ^{2}D NMR spectra, $\Delta\nu$ vs. T [90Mac]. $\Delta\nu$: quadrupole splitting between the singularities of the spectra. ν_L = 30.7 MHz. Polycrystalline specimens. The estimated rate of deuteration was more than 99%.

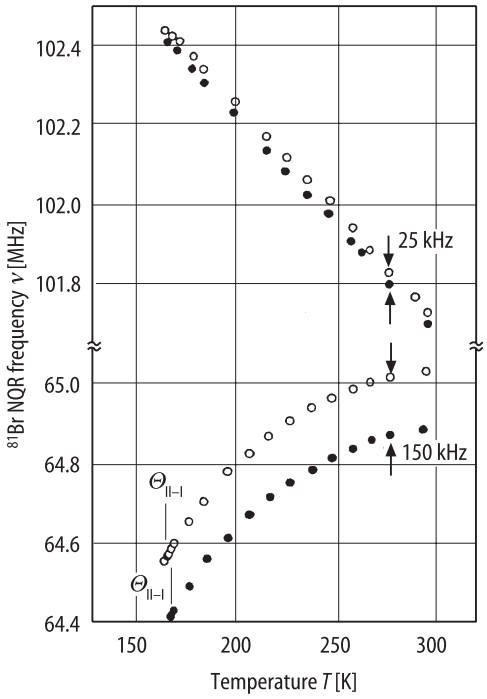

Fig. 56A-4-012. $(CH_3NH_3)_3Sb_2Br_9$, $(CH_3ND_3)_3Sb_2Br_9$. ν vs. T in phase I [90Mac]. ν: ^{81}Br NQR frequency. Full circle: $(CH_3NH_3)_3Sb_2Br_9$, open circle: $(CH_3ND_3)_3Sb_2Br_9$. Polycrystalline specimens. The estimated rate of deuteration was more than 99%. The frequency shift of the upper branch on deuteration and that of the lower one was 25 kHz and 150 kHz, respectively, as shown by arrows.

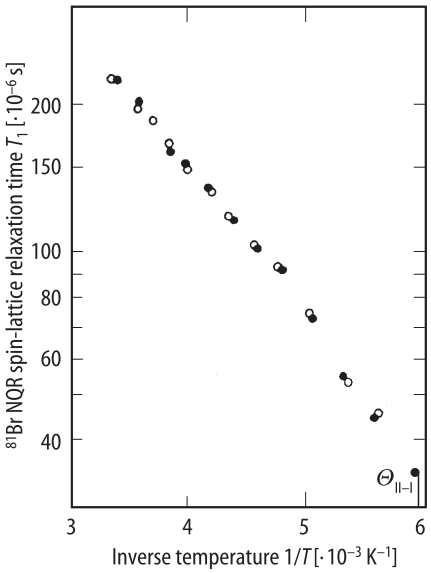

Fig. 56A-4-013. $(CH_3NH_3)_3Sb_2Br_9$, $(CH_3ND_3)_3Sb_2Br_9$. T_1 vs. $1/T$ in phase I [90Mac]. T_1: ^{81}Br NQR spin-lattice relaxation time. Full circle: $(CH_3NH_3)_3Sb_2Br_9$, open circle: $(CH_3ND_3)_3Sb_2Br_9$. The estimated rate of deuteration was more than 99%.

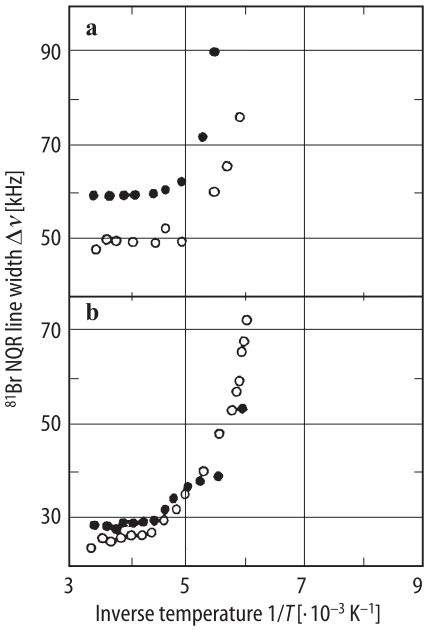

Fig. 56A-4-014. $(CH_3NH_3)_3Sb_2Br_9$, $(CH_3ND_3)_3Sb_2Br_9$. $\Delta\nu$ vs. $1/T$ in phase I [90Mac]. $\Delta\nu$: ^{81}Br NQR line width. Full circle: $(CH_3NH_3)_3Sb_2Br_9$, open circle: $(CH_3ND_3)_3Sb_2Br_9$. (**a**) upper frequency line, (**b**) lower frequency line. The upper and lower lines correspond to those shown in Fig. 56A-4-012. The estimated rate of deuteration was more than 99 %.

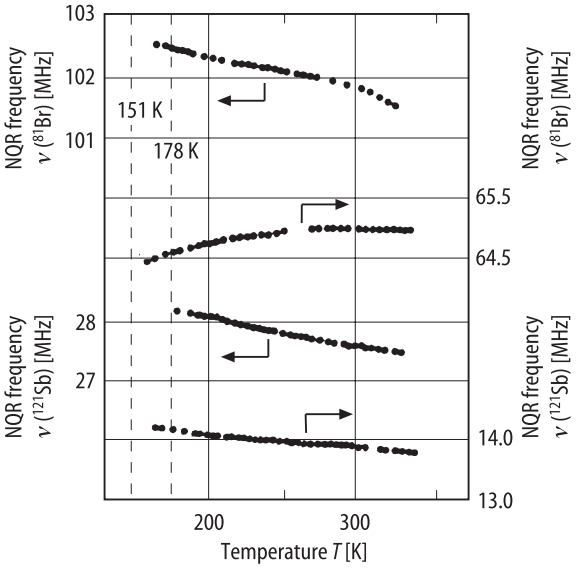

Fig. 56A-4-015. $(CH_3NH_3)_3Sb_2Br_9$. ν vs. T in phase I [92Ish]. ν: ^{121}Sb and ^{81}Br NQR frequencies.

References

85Jak Jakubas, R., Galewski, Z., Sobczyk, L., Matuszewski, J.: J. Phys. C **18** (1985) L857.

86Jak Jakubas, R., Miniewicz, A.: Ferroelectrics **70** (1986) 145.

90Koz Kozioł, P., Jakubas, R.: Phys. Status Solidi (a) **120** (1990) K93.

90Mac Maćkowiak, M., Weiden, N., Weiss, A.: Phys. Status Solidi (a) **119** (1990) 77.

92Ish Ishihara, H., Watanabe, K., Iwata, A., Yamada, K., Kinoshita, Y., Okuda, T., Krishnan, V.G., Dou, S., Weiss, A.: Z. Naturforsch. **47a** (1992) 65.

92Jak Jakubas, R., Lefebvre, J., Fontaine, H., François, P.: Solid State Commun. **81** (1992) 139.

93Jak Jakubas, R., Bator, G., Baran, J.: J. Phys. Chem. Solids **54** (1993) 1065.

94Jak Jakubas, R., Bator, G., Sobczyk, L., Mróz, J.: Ferroelectrics **158** (1994) 43.

94Mro Mróz, J., Jakubas, R.: Ferroelectrics Lett. **17** (1994) 73.

No. 56A-5 $(CH_3NH_3)_3Bi_2Br_9$, Methylammonium nonabromodibisumuthate

(M = 1233.29)

1a Ferroelectric activity in $(CH_3NH_3)_3Bi_2Br_9$ was discovered by Jakubas et al. in 1988. 88Jak

b

phase	IV	III	II	I	88Jak
state	F			P	
crystal system				trigonal	
space group				$P\bar{3}ml - D_{3d}^3$	88Jak
Θ [K]	104		142	190	92Jak

Ferroelectric axis is most probably along the a axis for hexagonal cell. 88Jak
Yellow in color. Cleavage plane perpendicular to the c axis for hexagonal cell. 88Jak
Phase diagram in regard to p: Fig. 56A-5-001.
$\rho = 3.30 \cdot 10^3$ kg m^{-3}, $\rho_X = 3.506(1) \cdot 10^3$ kg m^{-3}. 92Ish

2a Crystal growth: slow evaporation of an aqueous solution of CH_3NH_3Br and $BiBr_3$ at the stoichiometric molar ratio with a great excess of HBr. 92Jak
See also 88Jak

b Crystal form: hexagonal plate. 88Jak

3a Unit cell parameters: a = 8.210(1) Å, c = 10.004(1) Å for hexagonal cell at 300 K. 92Ish

b Z = 1 in phase I. 88Jak
Crystal structure: Fig. 56A-5-002.
Positional and temperature parameters: Table 56A-5-001.
Interatomic distances and bond angles: Table 56A-5-002.

4 Thermal expansion: Fig. 56A-5-003.

5a Dielectric constant: Fig. 56A-5-004, Fig. 56A-5-005, Fig. 56A-5-006, Fig. 56A-5-007, Fig. 56A-5-008.
Dielectric dispersion: Fig. 56A-5-009, Fig. 56A-5-010, Fig. 56A-5-011, Fig. 56A-5-012, Fig. 56A-5-013.

c Spontaneous polarization: Fig. 56A-5-014, Fig. 56A-5-015, Fig. 56A-5-016.

8a Elastic stiffness: Fig. 56A-5-017.

9a Infrared transmission: see 93Jak2

10a Raman scattering: see 94Min

13a NMR: Fig. 56A-5-018, Fig. 56A-5-019.
NQR: Fig. 56A-5-020.

15b Domain structure: see 90Mro, 94Jak

Table 56A-5-001. $(CH_3NH_3)_3Bi_2Br_9$. Crystal structure of phase I [92Ish]. Fractional coordinates and mean square displacement $\overline{u^2}$. $\overline{u^2}$ [$\cdot 10^{-4}$ Å^2] is defined by $B/(8\pi^2)$, where B is defined by Eq. (e) in Introduction. T = 300 K. Dummy K atoms were used instead of the $CH_3NH_3^+$, because the latter one execute isotropic rotation at RT and K atoms are isoelectric to $CH_3NH_3^+$.

Atom	Position	x	y	z	$\overline{u^2}$
Bi	2d	0.6667	0.3333	0.1948(15)	131(39)
Br(1)	3e	0.5000	0.5000	0.0000	613(140)
Br(2)	6i	0.3235(26)	0.1617	0.3285(24)	557(68)
K(1) [a])	1a	0.0000	0.0000	0.0000	2181(792)
K(2) [a])	2d	0.6667	0.3333	0.6839(139)	3862(603)

[a]) These K atoms are used as dummy atoms for the refinement.

Table 56A-5-002. $(CH_3NH_3)_3Bi_2Br_9$. Crystal structure of phase I [92Ish]. Bond distances [Å] and angles [°]. T = 300 K.

Bi–Br(1) [a])	3.069(15)
Bi–Br(2) [b])	2.783(33)
Bi–Br(1)–Bi(1^{i}) [c])	180.0
Br(2)–Bi–Br(2^{ii})	98.8(9)
Br(1)–Bi–Br(2)	88.1(7)
Br(1)–Bi–Br(1^{iii})	84.0(4)
Br(1)–Bi–Br(2^{ii})	169.3(9)

[a]) The bridging bromine atom.
[b]) The terminal bromine atom.
[c]) Atoms carrying i, ii, and iii are related by the relationships
2/3, 1/3, $\bar{z} \rightarrow$ 1/3, 2/3, z; 2 x, x, $\bar{z} \rightarrow \bar{x}$, x, $\bar{z}$;
and 1/2, 1/2, 0 → 1/2, 0, 0, respectively.

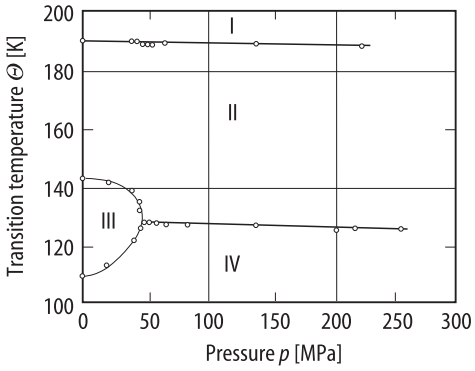

Fig. 56A-5-001. $(CH_3NH_3)_3Bi_2Br_9$. Θ vs. p [89Koz].

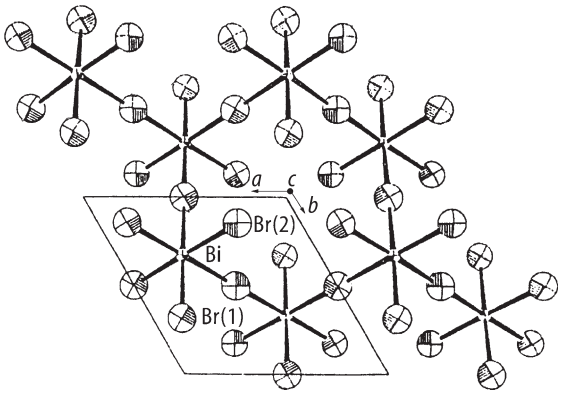

Fig. 56A-5-002. $(CH_3NH_3)_3Bi_2Br_9$. Structure of phase I [92Ish]. View along the c axis, showing layer structure of anion lattice. T = 300 K.

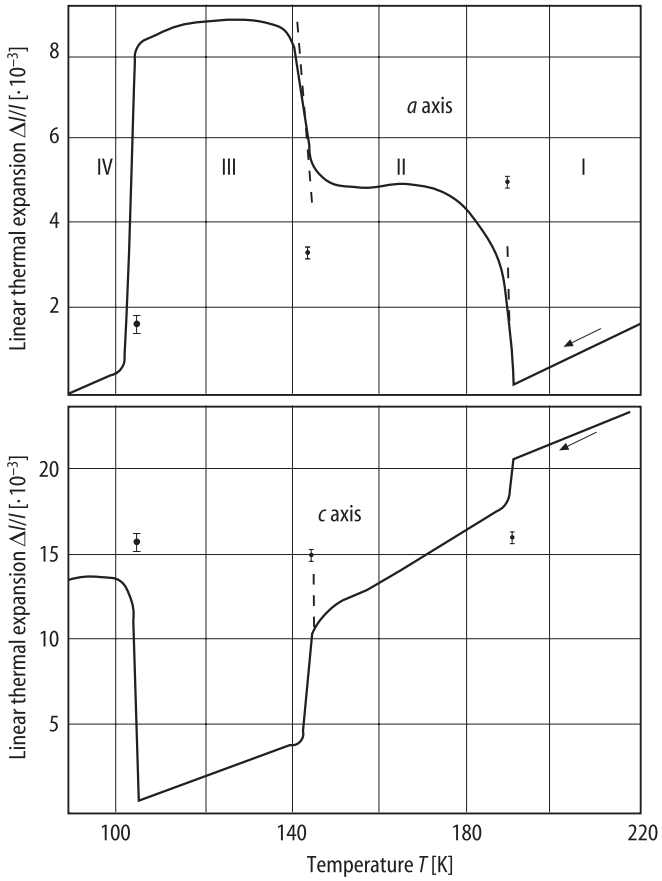

Fig. 56A-5-003. $(CH_3NH_3)_3Bi_2Br_9$. $\Delta l/l$ vs. T [92Jak]. Upper figure is along the *a* axis, lower one along the *c* axis.

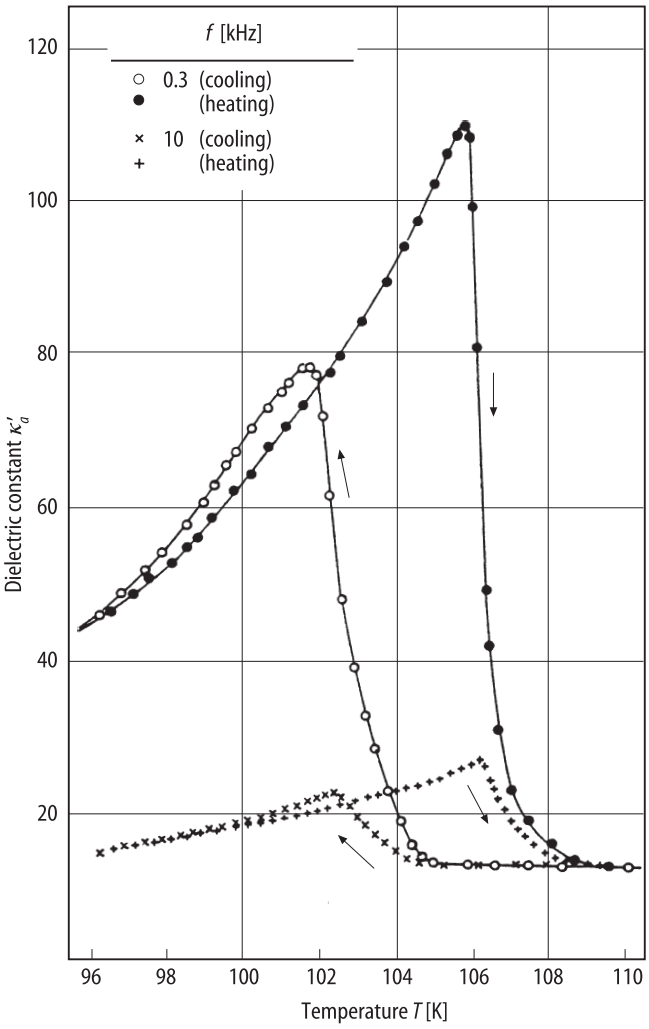

Fig. 56A-5-004. $(CH_3NH_3)_3Bi_2Br_9$. κ'_a vs. T in the vicinity of Θ_{IV-III} [88Jak]. Parameter: f.

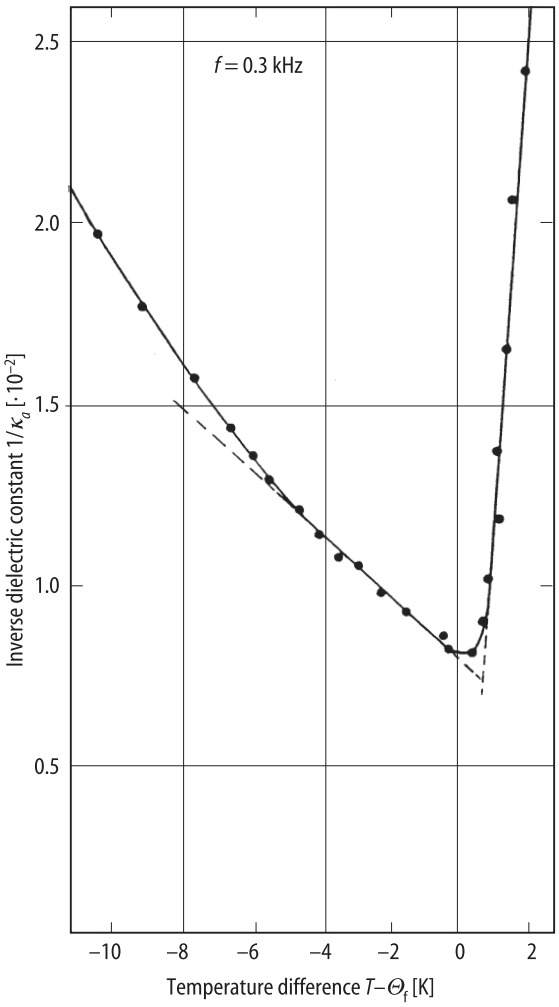

Fig. 56A-5-005. $(CH_3NH_3)_3Bi_2Br_9$. $1/\kappa_a$ vs. $T - \Theta_f$ [88Jak].

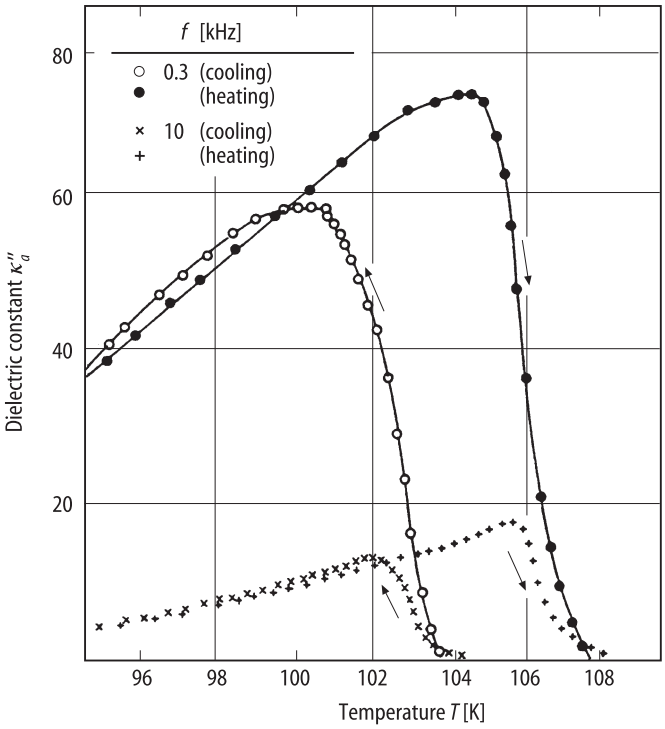

Fig. 56A-5-006. $(CH_3NH_3)_3Bi_2Br_9$. κ_a'' vs. T in the vicinity of Θ_{IV-III} [88Jak]. Parameter: f.

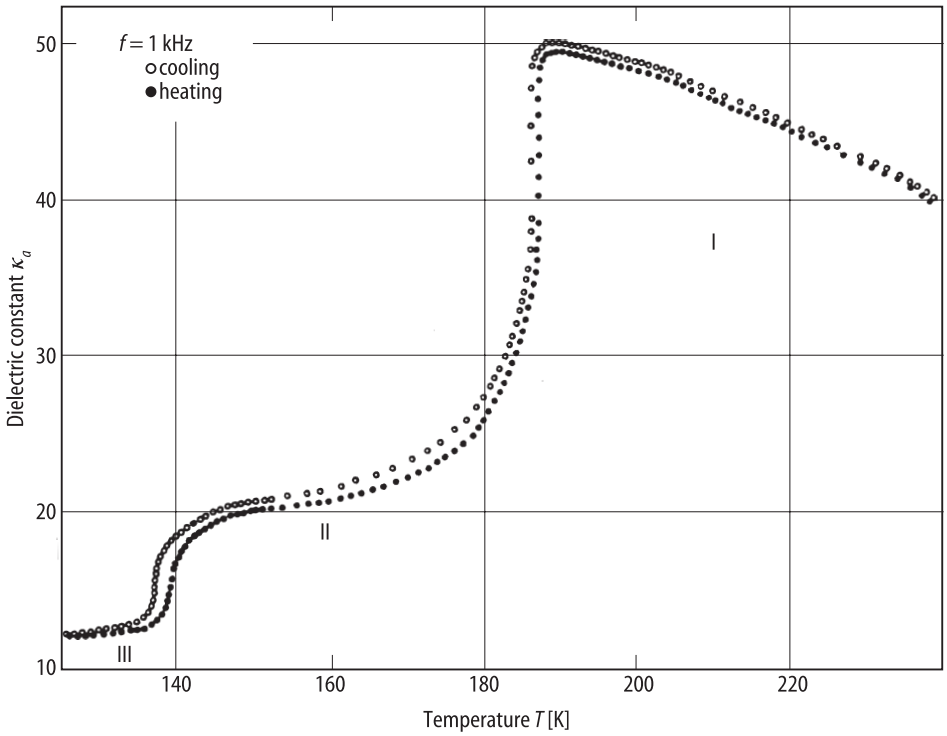

Fig. 56A-5-007. $(CH_3NH_3)_3Bi_2Br_9$. κ_a vs. T [88Jak].

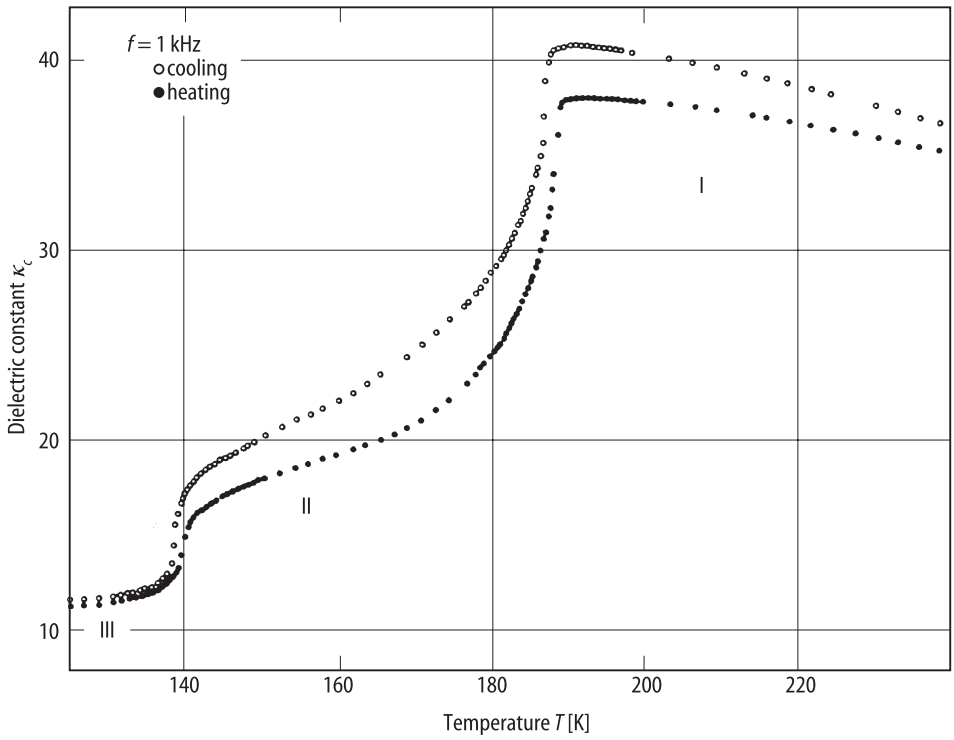

Fig. 56A-5-008. $(CH_3NH_3)_3Bi_2Br_9$. κ_c vs. T [88Jak].

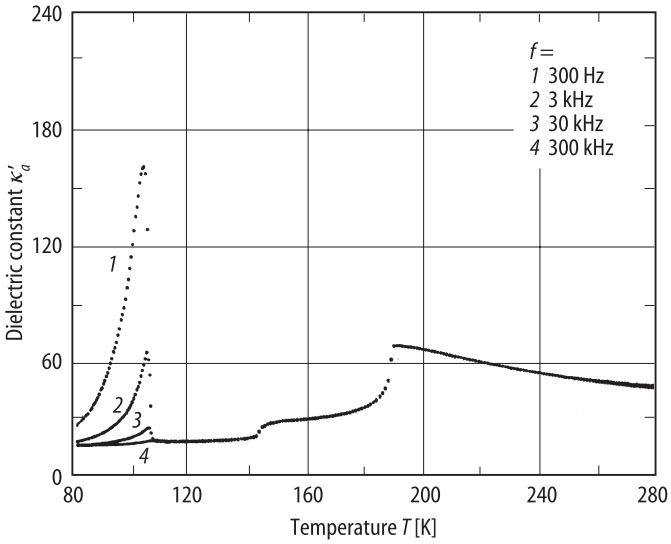

Fig. 56A-5-009. $(CH_3NH_3)_3Bi_2Br_9$. κ'_a vs. T [93Iwa]. Parameter: f.

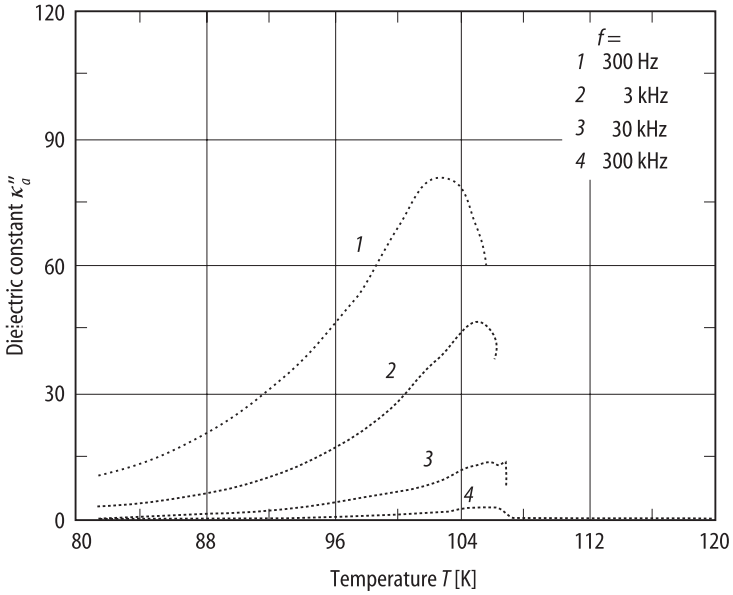

Fig. 56A-5-010. $(CH_3NH_3)_3Bi_2Br_9$. κ_a'' vs. T [93Iwa]. Parameter: f.

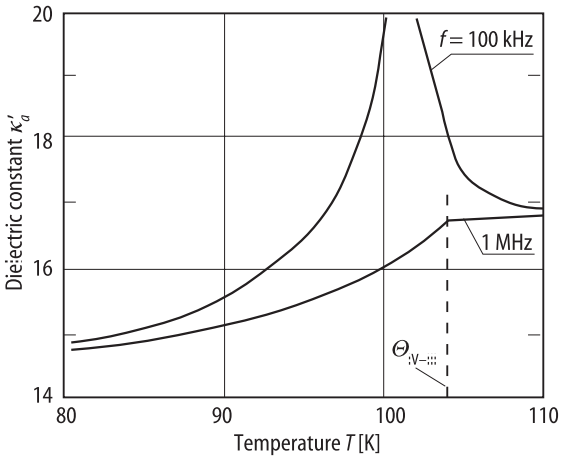

Fig. 56A-5-011. $(CH_3NH_3)_3Bi_2Br_9$. κ_a' vs. T [94Jak]. Parameter: f.

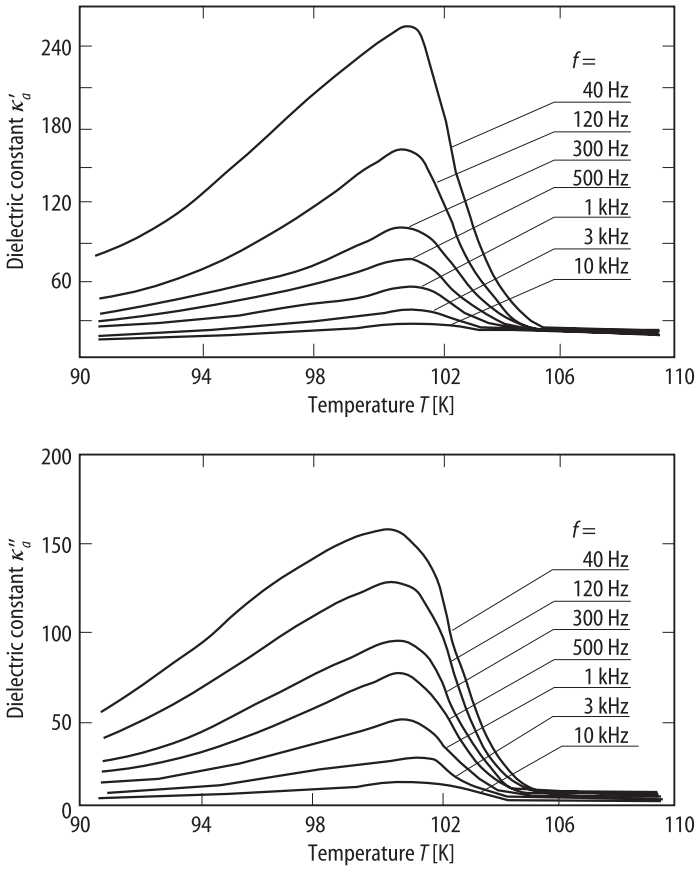

Fig. 56A-5-012. $(CH_3NH_3)_3Bi_2Br_9$. κ_a', κ_a'' vs. T [93Jak1]. Parameter: f in a range of 40 Hz...10 kHz.

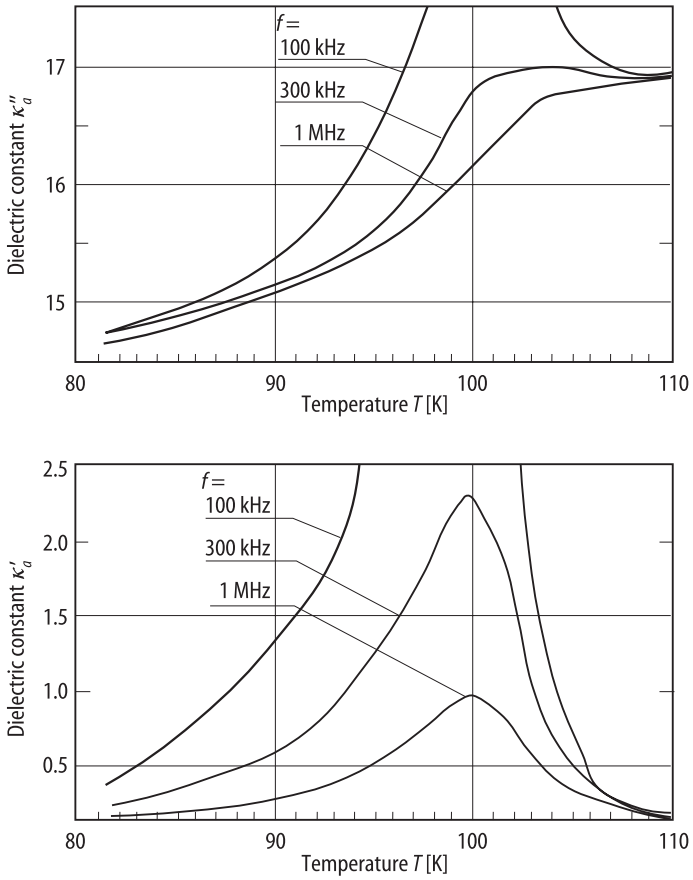

Fig. 56A-5-013. $(CH_3NH_3)_3Bi_2Br_9$. κ_a', κ_a'' vs. T [93Jak1]. Parameter: f in a range of 100 kHz...1 MHz.

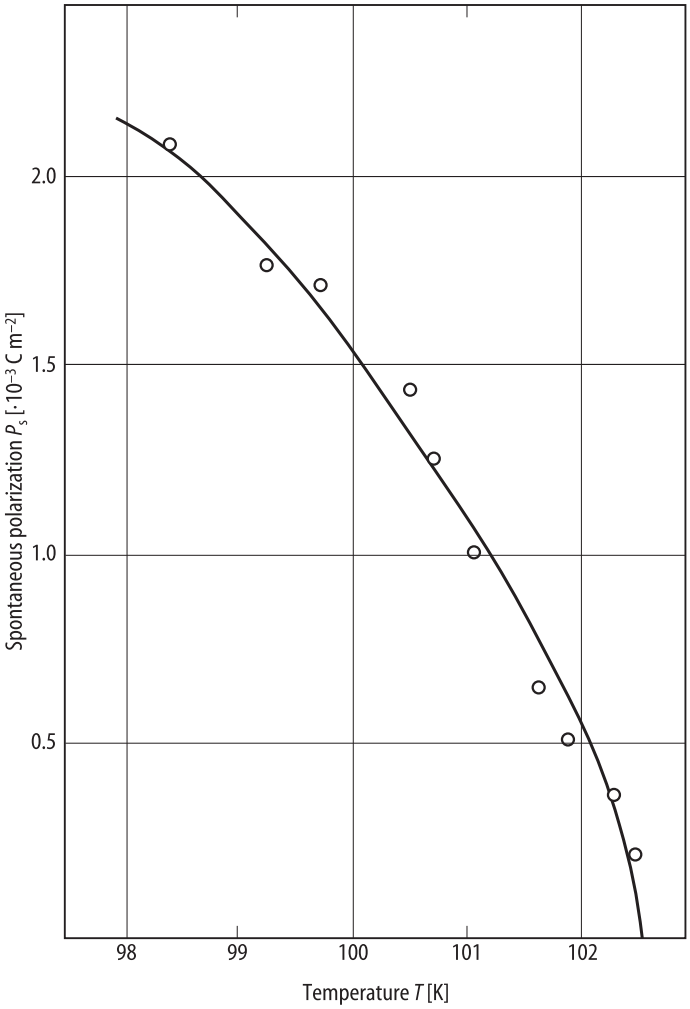

Fig. 56A-5-014. $(CH_3NH_3)_3Bi_2Br_9$. P_s vs. T [88Jak]. P_s: spontaneous polarization along the *a* axis.

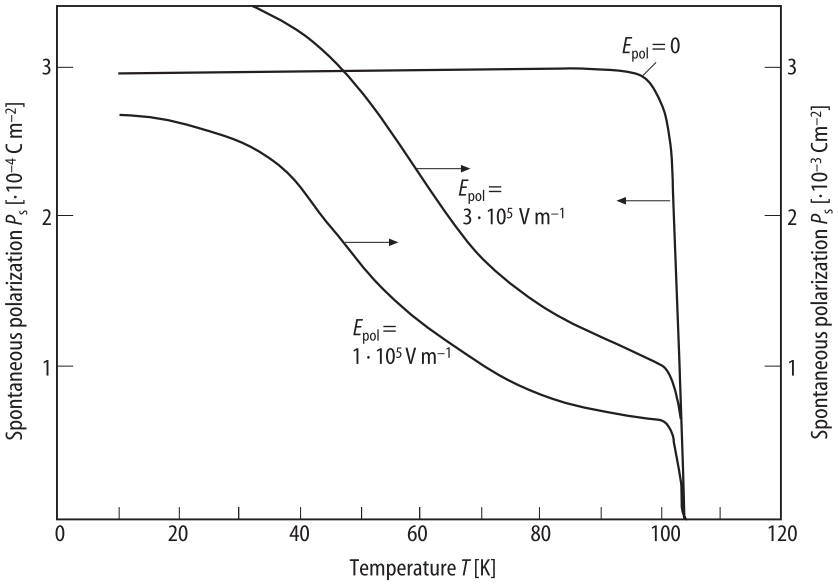

Fig. 56A-5-015. $(CH_3NH_3)_3Bi_2Br_9$. P_s vs. T [93Jak1]. P_s: spontaneous polarization along the a axis. Parameter: E_{pol}. E_{pol}: poling field.

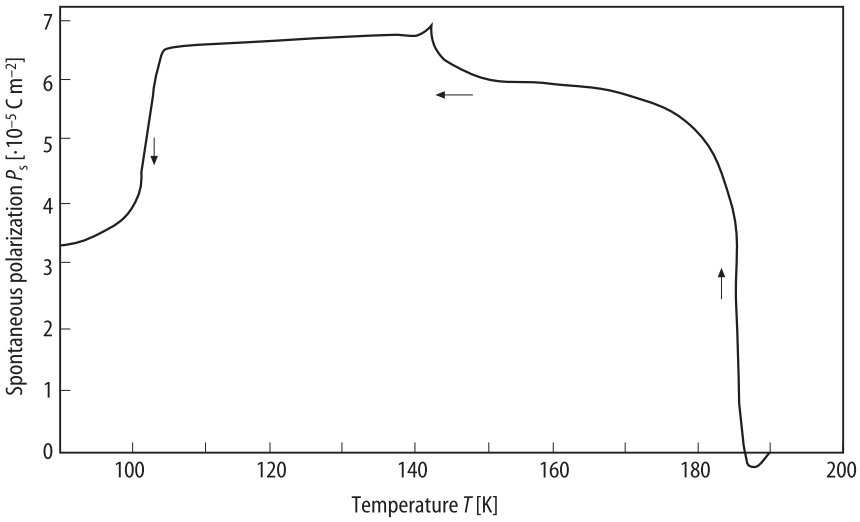

Fig. 56A-5-016. $(CH_3NH_3)_3Bi_2Br_9$. P_s vs. T [90Mro]. P_s: spontaneous polarization along the c axis.

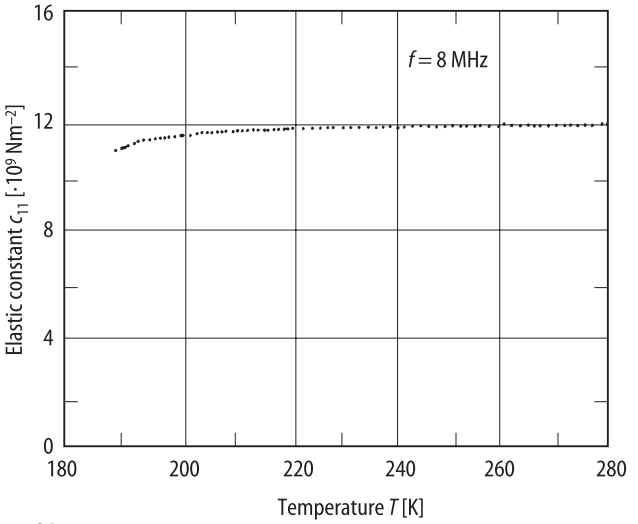
f = 8 MHz
Elastic constant c_{11} [·10⁹ Nm⁻²]
16
12
8
4
0
180
200
220
240
260
280
Temperature T [K]

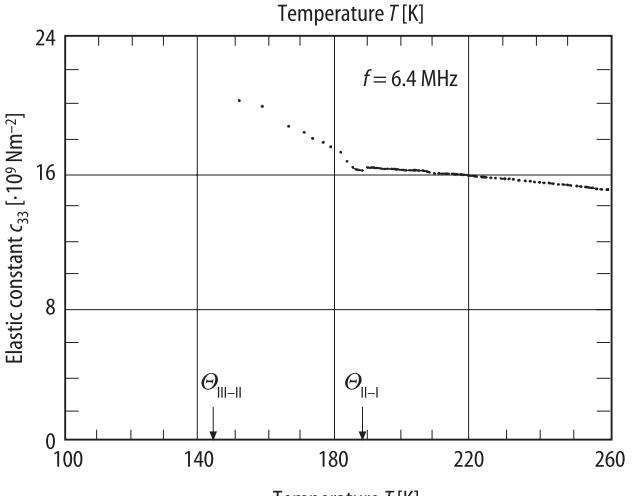
f = 6.4 MHz
Elastic constant c_{33} [·10⁹ Nm⁻²]
24
16
8
0
Θ_{III-II}
Θ_{II-I}
100
140
180
220
260
Temperature T [K]

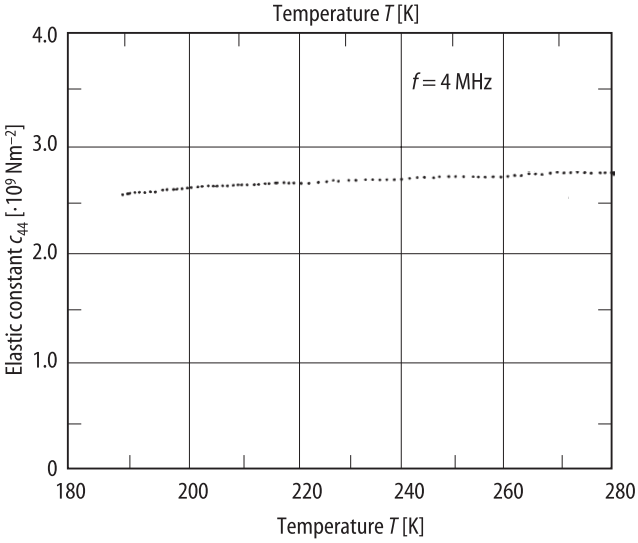
f = 4 MHz
Elastic constant c_{44} [·10⁹ Nm⁻²]
4.0
3.0
2.0
1.0
0
180
200
220
240
260
280
Temperature T [K]

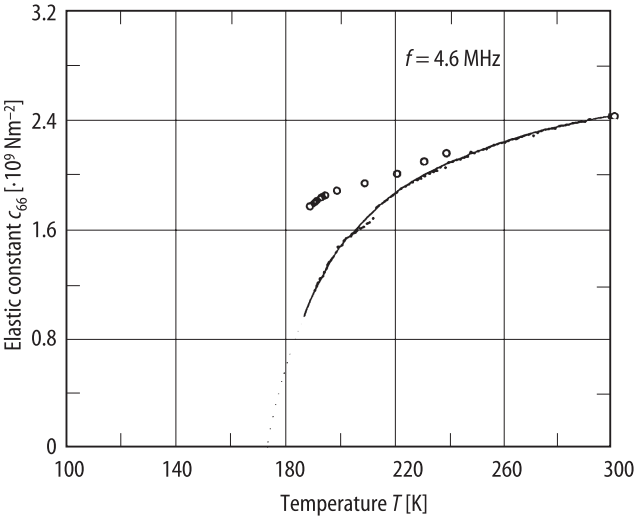

Fig. 56A-5-017. $(CH_3NH_3)_3Bi_2Br_9$. c_{ii} vs. T [93Iwa]. c_{ii}: elastic stiffness constant.

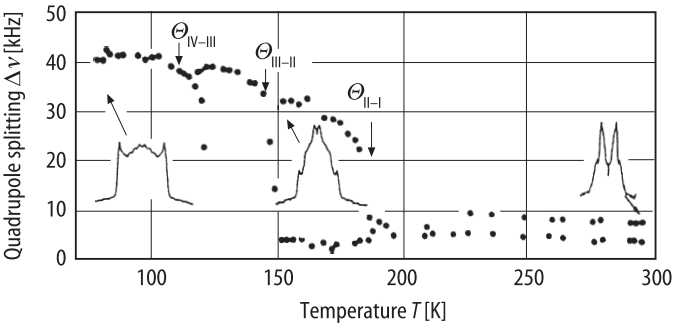

Fig. 56A-5-018. $(CH_3ND_3)_3Bi_2Br_9$. ^{2}D NMR spectra, $\Delta\nu$ vs. T [92Ish]. $\Delta\nu$: quadrupole splitting between the singularities of the spectra. ν_L = 22.00 MHz. The lateral scale of the spectrum of phase I is expanded by a factor of 2.5.

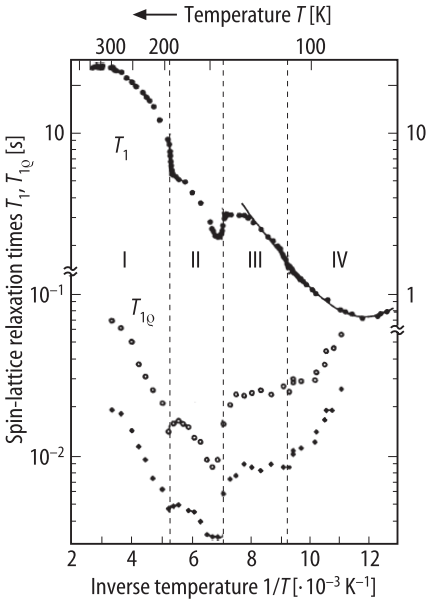

Fig. 56A-5-019. $(CH_3NH_3)_3Bi_2Br_9$. T_1, $T_{1\rho}$ vs. $1/T$ [91Koz]. T_1 and $T_{1\rho}$ are spin-lattice relaxation times of proton in laboratory frame and rotating frame, respectively. ν_L = 42 MHz for T_1, 32 MHz for $T_{1\rho}$. The B fields applied for $T_{1\rho}$ were 10^{-3} T (open circle) and $5 \cdot 10^{-4}$ T (full lozenge), respectively.

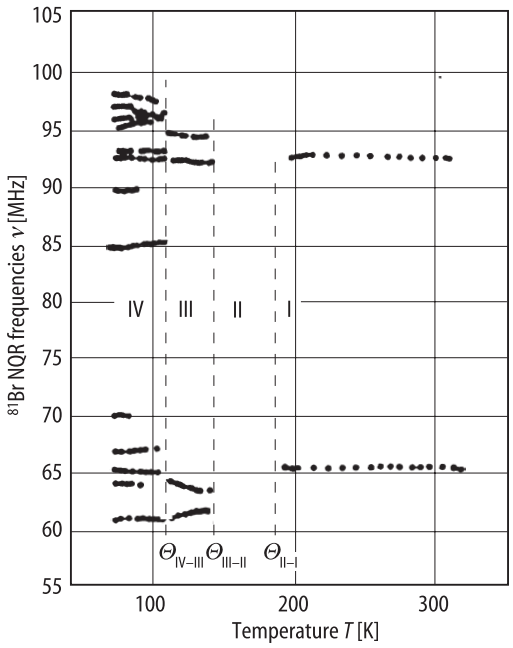

Fig. 56A-5-020. $(CH_3NH_3)_3Bi_2Br_9$. ν vs. T [92Ish]. ν: ^{81}Br NQR frequencies.

References

88Jak Jakubas, R., Krzewska, U., Bator, G., Sobczyk, L.: Ferroelectrics **77** (1988) 129.

89Koz Kozioł, P., Jakubas, R.: Solid State Commun. **72** (1989) 143.

90Mro Mróz, J., Czapla, Z., Jakubas, R.: Acta Phys. Pol. A **77** (1990) 501.

91Koz Kozioł, P., Furukawa, Y., Nakamura, D.: J. Phys. Soc. Jpn. **60** (1991) 3850.

92Ish Ishihara, H., Watanabe, K., Iwata, A., Yamada, K., Kinoshita, Y., Okuda, T., Krishnan, V.G., Dou, S., Weiss, A.: Z. Naturforsch. **47a** (1992) 65.

92Jak Jakubas, R., Lefebvre, J., Fontaine, H., François, P.: Solid State Commun. **81** (1992) 139.

93Iwa Iwata, M., Eguchi, M., Ishibashi, Y., Sasaki, S., Shimizu, H., Kawai, T., Shimanuki, S.: J. Phys. Soc. Jpn. **62** (1993) 3315.

93Jak1 Jakubas, R., Bator, G., Mróz, J.: Ferroelectrics **146** (1993) 65.

93Jak2 Jakubas, R., Bator, G., Baran, J.: J. Phys. Chem. Solids **54** (1993) 1065.

94Jak Jakubas, R., Bator, G., Sobczyk, L., Mróz, J.: Ferroelectrics **158** (1994) 43.

94Min Miniewicz, A., Jakubas, R., Ecolivet, C., Girard, A.: J. Raman Spectrosc. **25** (1994) 371.